

1 Paleoseismic history of the intermountain Rieti Basin (Central 2 Apennines, Italy)

3 Franz A. Livio¹, Anna M. Blumetti², Valerio Comerci², Maria F. Ferrario¹, Gilberto Binda⁴, Marco
4 Caciagli³, Michela Colombo¹, Pio Di Manna², Fernando Ferri², Fiorenzo Fumanti², Roberto Gambillara¹,
5 Maurizio Guerra², Luca Guerrieri², Paolo Lorenzoni⁵, Valerio Materni⁶, Francesco Mischione², Rosa
6 Nappi⁷, Rosella Nave⁷, Kathleen Nicoll⁸, Alba Peiro⁹, Marco Pizza¹, Roberto Pompili², Luca M. Puzzilli²,
7 Mauro Roma², Aurora Rossi¹, Valerio Ruscito², Vincenzo Sapia⁶, Argelia Silva Fragoso¹, Emanuele
8 Scaramuzzo¹, Frank Thomas¹, Giorgio Tringali¹, Stefano Urbini⁶, Andrea Zerboni¹⁰, Alessandro M.
9 Michetti^{1,7}

10
11 ¹Università degli Studi dell’Insubria, Como, Italy

12 ²ISPRA, Geological Survey of Italy, Roma, Italy

13 ³Istituto Nazionale di Geofisica e Vulcanologia, Sezione di Bologna, Italy

14 ⁴Norwegian Institute for Water Research, Oslo, Norway

15 ⁵Professional Soil Science Consultant, Rieti, Italy

16 ⁶Istituto Nazionale di Geofisica e Vulcanologia, Sezione di Roma 2, Italy

17 ⁷Istituto Nazionale di Geofisica e Vulcanologia, Osservatorio Vesuviano, Napoli, Italy

18 ⁸University of Utah, Salt Lake City, Utah USA

19 ⁹University of Zaragoza, Spain

20 ¹⁰Università degli Studi di Milano, Italy

21 *Correspondence to:* F.A. Livio (franz.livio@uninsubria.it)

22 **Abstract.** From the paleoseismological and seismotectonic point of view, the intermountain basins of the Central Apennines
23 of Italy are one of the most studied areas worldwide. Within this context, however, the Rieti Basin, bounded at its sides by
24 active normal faults and with its peculiar rhombohedral shape, is a relatively overlooked area, and its most recent
25 paleoseismological studies date back to the ‘90s. This is a key area both for completing the paleoseismological history of this
26 sector of the chain and for understanding how the present-day extensional regime is accommodated through time by the faults
27 bounding the basin. With this aim in mind, we excavated 17 paleoseismological trenches along the normal faults bordering the
28 Rieti Basin (Central Apennines, Italy) and unveiled at least 6 paleoearthquakes that ruptured the faults during the last ca. 20
29 kyr.

30 Our analysis of the paleoearthquake succession along the basin-bounding faults suggests that a spatial pattern is followed
31 during sequences of rupturing events, with a maximum credible earthquake of Mw 6.5, consistently within this sector of the
32 Central Apennines.

33 **1 Introduction**

34 The Central Apennines in Italy are among the best studied areas worldwide in terms of active tectonics and paleoseismology
35 (Michetti et al., 1996; Pantosti et al., 1996; Galadini and Galli, 1999; Salvi et al., 2003; Roberts and Michetti, 2004; Galli et
36 al., 2008, 2011; Gori et al., 2015; Moro et al., 2016; Blumetti et al., 2017; Di Domenica and Pizzi, 2017; Cinti et al., 2018;
37 Iezzi et al., 2019, 2023; Roberts et al., 2025). Tens of paleoseismological trenches have been excavated along the active normal
38 faults of this mountain belt, providing one of the world's most complete datasets for an extensional domain, together with the
39 well-known Basin and Range Province of the western U.S. (McCalpin, 2009). This led to choosing the Italian Central
40 Apennines as one important global case study for the development of codes for fault-based seismic hazard assessment (Faure
41 Walker et al., 2021; Scotti et al., 2021).

42 Nonetheless, some overlooked areas within the Central Apennines lack comprehensive studies and investigations. This is the
43 case of the Rieti Basin (Fig. 1), an intermountain fault-bounded depression located in the axial sector of the range. Following
44 the contractional events that built the chain, the Rieti area experienced several phases of extensional tectonics during the Plio-
45 Quaternary, leading to the present day-configuration. Today, the Rieti Basin morphology appears as a box-shaped alluvial
46 plain, bounded by normal faults striking almost orthogonally to each other (Fig. 1). The master fault of the basin ("Rieti Fault";
47 Roberts and Michetti, 2004, and references therein) is the ca. 21 km long Eastern Border Fault (Fig. 1). The Rieti Fault is part
48 of a belt of active Quaternary normal faults (including the nearby Fiamignano and Fucino Faults; Bosi, 1975; Michetti et al.,
49 1996; Mildon et al., 2022) that characterizes the western side of the Central Apennines (Cowie and Roberts, 2001).

50 Past research focused on the Plio-Quaternary tectono-sedimentary evolution of the basin (Cavinato, 1993; Calderini et al.,
51 1998; Cavinato et al., 2000, 2002; Guerrieri et al., 2006), but only a few studies from the mid-90s, revealed Late Pleistocene
52 to Holocene strong seismic events by means of a paleoseismological approach. Observed Holocene slip rates at Piedicolle and
53 La Casetta Sites are in the order of 0.2 - 0.4 mm/yr. This is in good agreement with slip-rates measured along post-glacial
54 bedrock fault scarps (Cowie and Roberts, 2001), and long-term slip rates estimated from displacement of Early Pleistocene
55 paleo-surfaces (e.g., Brunamonte et al., 1993; Michetti et al., 1995). In fact, some open questions are still pending on the area,
56 including: i) the real seismotectonic potential of the Rieti Basin faults; ii) the coexistence and contemporary activity of two
57 sets of ca. orthogonal normal faults under the same extensional domain; and iii) the possible occurrence of earthquakes
58 rupturing the whole length of the Rieti Fault.

59 In 2020-2022, the Italian Government Extraordinary Commissioner for the 2016 Central Italy post-earthquake reconstruction
60 funded a program of studies on faults affecting urbanized zones in the earthquake epicentral areas. Some of the inhabited
61 centers under study are located along the northern, eastern and southern borders of the Rieti intermountain basin; boxes in
62 Figure 1C show the selected Study Areas. In 2021 and 2022, our team discovered evidence of Late Pleistocene and Holocene
63 activity along the investigated faults from study of 17 new paleoseismic trenches with 52 radiometric dates, and extensive
64 geophysical prospecting. We describe trench siting and investigations on the three sides of the basin, identifying several
65 paleoearthquakes that occurred in the last about 20 kyr. Based on these data, the paper aims at providing a summary of the

66 paleoseismic history of the Rieti basin; we discuss Late Quaternary fault slip-rates, event chronology, and we present a
67 space-time paleoseismological diagram to infer the possible sequence of single vs multi-rupture events that affected the
68 basin.

69 **2 Geological and seismotectonic setting**

70 The Rieti Basin is within the Central Apennines, a former Meso-Cenozoic passive margin that evolved in a fold and thrust belt
71 during the Neogene westward subduction of the Adriatic plate. The present-day setting is the result of an eastward progressive
72 migration of the front of the accretionary wedge and of the back-arc extensional domain (Doglioni, 1991; Cavinato and De
73 Celles, 1999; Cosentino et al., 2010), with the axial sector of the mountain chain currently affected by strong normal fault
74 earthquakes due to active crustal extension (Fig. 1b).

75 The local paleogeographic domain is the Umbria-Marche Domain: a stack of tectonic units composed of Jurassic-Paleogene
76 carbonate successions (i.e., the Mt. Sabini and Mt. Reatini units; Fig. 1c). The thrust sheets superposed on an inherited tectonic
77 setting developed during Jurassic-Eocene rifting of the passive margin (Galluzzo and Santantonio, 2002; Santantonio and
78 Carminati, 2011; Capotorti and Muraro, 2024), which was characterized by mainly N-S striking normal faults but locally
79 represented by a dense grid of faults, also including ca. E-W and NW-SE normal faults (Capotorti and Muraro, 2024).

80 Presently, the Rieti Basin is a box-shaped morphological depression, bounded along all its sides by Quaternary normal faults.
81 The development and evolution of the basin is closely related to the extensional regime that affected the western flank of the
82 eastward migrating Apennine chain during the Quaternary (Calderini et al., 1998; Cavinato and De Celles, 1999; Cavinato et
83 al., 2000, 2002; Roberts and Michetti, 2004; Guerrieri et al., 2006), in combination with regional uplifting (Dramis, 1992;
84 Galadini et al., 2003). During the Early Pleistocene, the subsidence of the basin was controlled by the eastern border normal
85 fault, striking ca. NNW-SSE (Fig. 1c). This structure, connected to a small monogenetic volcano formed near Cupaello (Lustrino
86 et al., 2025), acted as the master-fault, controlling a progressive deepening of a half-graben and promoting the deposition of
87 thick alluvial fan deposits (i.e., the Fosso Canalicchio Synthem) and alluvial plain sequences (i.e., the Monteleone Sabino
88 Synthem), pinching out to the west. During the Middle Pleistocene, along the margins of the basin, the Early Pleistocene
89 deposits were displaced by a few hundred meters, with normal faulting slip rates in the order of 0.2 – 0.4 mm/yr (Michetti et
90 al., 1995), with further deepening of the Rieti Basin. Regional uplift triggered strong fluvial erosion from the Nera River,
91 which captured the Velino River through the Le Marmore threshold, and generated the northward diversion of the whole
92 hydrographic network (Guerrieri et al., 2006). Later tectonic events developed other sets of faults, some of them in the inner
93 portions of the basin, finally resulting in the orthogonal fault architecture presently bordering this intra-mountain depression.
94 Faults also controlled fluid flow and, together with climate oscillations, the deposition and erosion of thick sequences of
95 travertine, coincident with spring emergence and water flow mainly along the northern and southern border of the basin
96 (Carrara et al., 1992). The fast Holocene growth (ca. 160 m of vertical accretion) of the Le Marmore travertine platform
97 dammed the Velino River and caused alluvial overfilling in the Rieti Plain with sedimentation rates of ca. 3 mm/yr (Guerrieri

98 et al., 2006; Archer et al., 2019). Fluvial erosion and deposition processes are therefore one order of magnitude more efficient
99 than tectonic faulting in shaping the local landscape of the Rieti Basin.

100 As already mentioned, we focus on the three areas along the border faults as requested by the Government Commissioner. To
101 the east, we investigated the master fault in the Cantalice Study Area; to the north, we investigated the N border fault at the
102 Rivodutri Study Area; to the south, we studied the eastern sector of the S border fault, at the Rieti-Santa Rufina Study Area
103 (i.e., east of Rieti town; Fig. 1c). The extensive investigations conducted under the 2016 post-seismic reconstruction project
104 provide a unique opportunity for a comprehensive characterization of local paleoearthquake surface faulting.

105 The seismicity of the Rieti Basin shows two ancient destructive events. The oldest (Io = X MCS; Me = 6.4) occurred in 76
106 BCE, of which, however, information is only available for the city of Rieti (Guidoboni et al. 2018, 2019). The second strongest
107 event recorded here is the Dec. 1st, 1298, earthquake (Mw 6.26; Io = X MCS; Brunamonte et al., 1993; Rovida et al., 2022)
108 whose epicenter is tentatively located to the north of the basin. Of note, a foreshock event occurred only a day before in the
109 southern part of the basin (Mw = 4.4; Io = V-VI MCS).

110 Relevant M>6 earthquakes, with epicenters within 40 km from the Rieti Basin, are likely responsible for coseismic
111 environmental effects recorded in the Rieti Basin itself (Archer et al., 2019). These include events that occurred on Sept. 9th,
112 1349 (Valle del Salto, Fiamignano Fault, Me = 6.1; Bosi, 1975; Mildon et al., 2022), Oct. 15th, 1639 (Amatrice, Laga Fault,
113 Me = 6.2; Galli et al., 2017; Mildon et al., 2017) and Jan 14th, 1703 (Norcia Fault, Me = 6.7; Blumetti, 1995; Guidoboni et al.
114 2018, 2019; Galli et al., 2021).

115 Several moderate historical earthquakes hit the area during the last 3 centuries (Fig. 1 c; Rovida et al., 2022). The Oct. 9th,
116 1785 (Mw 5.76; Io VIII-IX MCS) hit to the northwest of the area. Two relatively recent moderate earthquakes occurred near
117 the N and S border faults, which we investigated with exploratory trenches (Fig. 1c). The one to the south is the June 27th,
118 1898, Santa Rufina event (Mw 5.5; Io VIII-IX MCS; Comerci et al., 2003) whose causative fault, based on the epicentral area,
119 could be either the eastern boundary fault or the southern boundary fault of the basin. A similar size earthquake hit the NE
120 border of the basin near Rivodutri on December 31st, 1948 (Mw 5.3; Io VIII MCS; Bernardini et al., 2013).

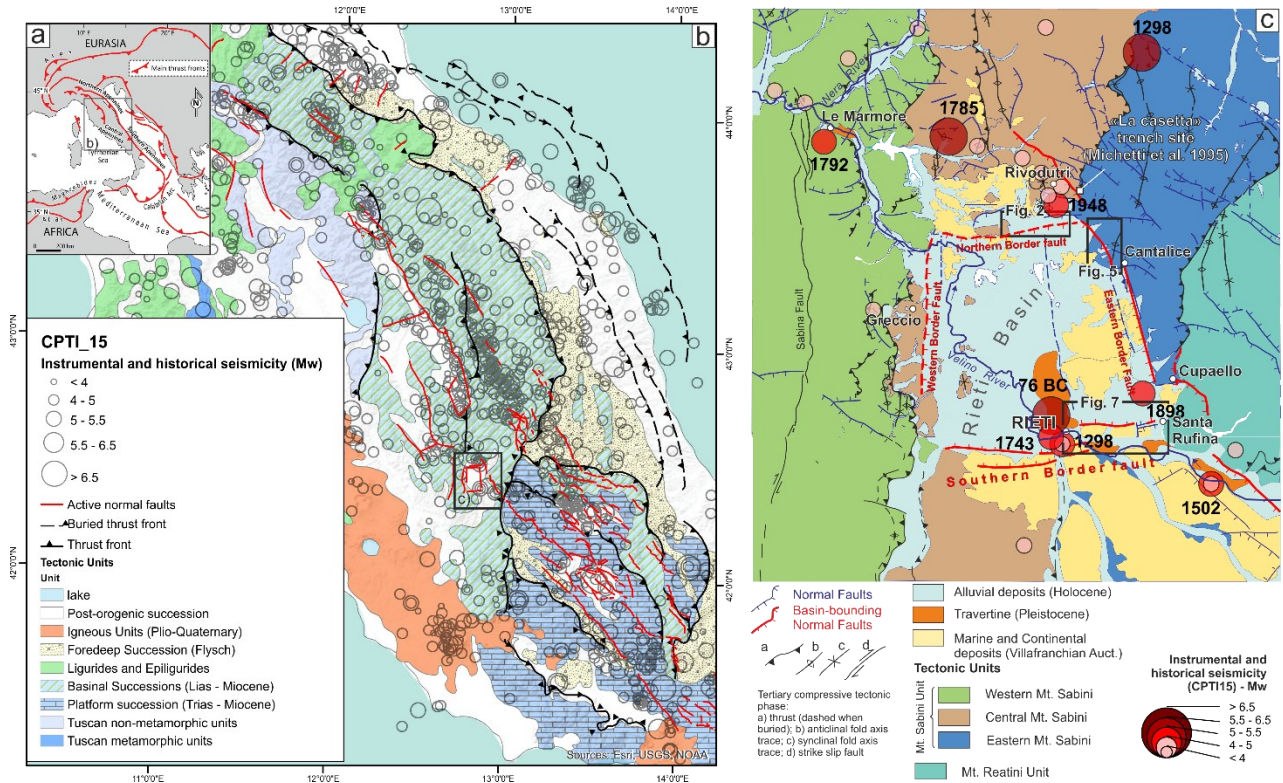


Figure 1: Geological setting: a) regional tectonic framework; b) simplified geological map of the Central Apennines with thrust fronts, the active normal faults running along the axis of the chain and seismicity (CPTI15 Catalogue, Rovida et al., 2022; CPTI5Med Catalogue, Guidoboni et al. 2018, 2019; and Baranello et al., 2024, for the 1743 Rieti earthquake); c) Rieti Basin area: simplified seismotectonic map (modified after Capotorti and Muraro, 2024; Servizio Geologico d'Italia, in press), the three Study Areas are delimited by boxes; note in the NW corner of the Figure, the Le Marmore travertine platform dams the Velino River Valley just before its confluence with the Nera River Valley, and therefore controls the drainage of the whole Rieti Plain.

3 Materials and Methods

We investigated the three Study Areas by means of a multidisciplinary approach that aimed for best imaging the border faults and locating the paleoseismological trenches. For the purposes of data description, in the following we divide the three investigated Areas (namely along the northern, eastern and southern Border Faults) into Sectors, each one containing multiple Sites (i.e., individual trenches).

Geophysical prospecting included Electric Resistivity Tomography (ERT) and Ground Penetrating Radar (GPR) imaging. We acquired ERT and GPR lines across the main strands of the border faults.

ERT data was acquired using alternatively i) the X612EM+ multichannel geo-resistivimeter (MAE - Molisana Apparecchiature Elettroniche s.r.l.) capable of handling 96 electrodes connected to 4 bidirectional 24-takeouts cables; ii) a Syscal R2 multichannel geo-resistivimeter (IRIS Instrument) capable of handling 64 electrodes connect to 4 cables (16-takeouts).

Regarding the investigation strategy, measurements were taken by using at least two out of three different arrays (i.e., among

139 Wenner, Wenner-Schlumberger, dipole-dipole and pole-dipole) along each profile, exploiting the different sensitivity of each
140 to achieve good resolution in both vertical and horizontal directions (see e.g. Dahlin & Zhou 2004). The sequences used during
141 the surveys always consisted of collecting a large number of measurements, as it was preferred to adopt a "high-resolution"
142 approach with an overabundant number of measurements for each layer/pseudo-depth. In particular, we used dipole-dipole
143 and/or pole-dipole arrays almost at each Site, as considered most suitable for characterizing areas where both lateral and
144 vertical variations in resistivity can be expected. This choice also made it possible to combine requirements for horizontal
145 measurement coverage, resolution, depth of investigation as well as needs related to timing and logistics (e.g., temporary
146 access to private areas). We carried out the 2D data inversion process after the quality check and data filtering using the
147 Res2DInv software by Geotomo (Loke & Barker 1996). For each profile, each dataset derived from single array was processed
148 individually and then, integrated into a single inversion process along with the others, to improve the quality of the final 2D
149 model that would be adopted and interpreted.

150 We acquired GPR lines with a GSSI Sir4000 instrument equipped by a 200 MHz antenna and coupled with a differential
151 GPS receiver Topcon GB1000 (post-processing kinematics) registering 1 position/sec. We summarize the acquisition as
152 follows: range: 150 ns; samples: 512; acquisition rate: 40 scan/s; dynamic: 32 bit. Data processing included vertical and
153 horizontal filtering, gain levelling, deconvolution and migration. We converted Two Way Traveltimes (TWT) to depth using
154 an average of dielectric constants calculated from diffraction hyperbolas occurring in the dataset and verified after the trench
155 excavations.

156 We logged the paleoseismological trenches at the 1:20 scale, using a reference net, and by means of digital photogrammetry.
157 For the latter, we used both portable LiDAR scanning (3D Scanner App for iOS) and a Structure from Motion and Multi-View
158 Stereo workflow (SfM-MvS – Metashape software; Westoby et al., 2012; Bemis et al., 2014). Field descriptions and horizon
159 designations followed internationally accepted guidelines (FAO, 2006), with the color definitions using nomenclature of the
160 Munsell® System (1994). We also carefully considered the sediments, horizons, boundaries and the crosscut relations with
161 structural features to chronologically constrain the progressive deformation affecting the stratigraphic sequences. Refer to the
162 Supplementary Material 2 for the trench photomosaics.

163 In the three Study Areas, we excavated 17 trenches, 13 of them suitable for paleoseismological analyses. We collected 52
164 samples for AMS dating, 21 from Rivodutri Municipality, 14 from Cantalice, 8 from Rieti and 9 from Santa Rufina
165 (Cittaducale). We mapped the position of the samples on the trench logs, while Table 1 shows a summary of all the dated
166 samples. The samples were analyzed by specialist laboratories (Beta Analytic and CEDAD); calibration was performed with
167 the INTCAL20 curve using the OxCal ver 3.10 or the BetaCal4.20 software (CEDAD and Beta samples, respectively).

168 We also took into account results from the Michetti et al. (1995) trenching at 3 sites (Piedicolle, La Casetta and Caporio).
169 Geochron Lab performed the radiocarbon dating of samples from these trenches; we revisited the original dates using the same
170 calibration methods as above. Please note that throughout the text below we always refer to the calibrated ages listed in the
171 last column of Table 1.

172 In the following text, we present results from individual trenches and ERT/GPR profiles that are most relevant for the
173 paleoseismological analysis. Please refer to the Supplementary Material, which includes information on all trenches and
174 geophysical prospecting realized during this project.

175 **4 Results**

176 We list the dated samples from the 13 paleoseismological trenches in Table 1, supplemented with the samples collected by
177 Michetti et al. (1995) in the La Casetta, Piedicolle and Caporio Sites. The Table presents both uncalibrated determinations and
178 calibrated age. In order to keep the discussion consistent and understandable, when the probability distribution of these
179 calibrated ages shows multiple peaks, in the following we will refer to the central age with the largest probability only (i.e.,
180 the one age calibration with highest probability; underlined in Table 1).

181

182 **Table 1: Summary of AMS dating results; we indicate the municipality and trench number, together with uncalibrated and**
183 **calibrated ages; “Dated Material” column abbreviations: “Org” for organic materials, “Charc” for charcoal, or burnt plant**
184 **materials; LTL samples are from CEDAD, CEntro di DATazione e Diagnostica, Università del Salento, Lecce; Beta samples are from**
185 **BETA Analytic, Inc., Miami.; GX samples (marked with *) are C14 dating after Michetti et al. (1995), recalibrated using the Oxcal**
186 **software and IntCal 20 curve; analyses from Geochron Lab., Cambridge, Massachusetts.**

Municipality	Trench	ID sample	ID lab	Dated material	Uncal age (years BP)	Calibrated age (years) using IntCal20 curve
Rivodutri	APO T2	C01	LTL21211	Org	223 ± 45	1522-1574 CE (5.9%) 1625-1698 CE (29.0%) <u>1722-1814 CE (38.4%)</u> 1835-1882 CE (3.8%) 1910 CE (18.3%)
		C03	LTL21259	Org	10947 ± 100	11127-10795 BCE (95.4%)
		C04	LTL21213	Org	6670 ± 45	<u>5664-5512 BCE (90.4%)</u> 5505-5481 BCE (5.0%)
		C06	LTL21214	Org	4404 ± 45	3327-3225 BCE (14.9%) 3183-3154 BCE (3.0%) <u>3110-2907 BCE (77.5%)</u>
		C07	LTL21215	Org	4868 ± 45	3767-3721 BCE (6.6%) <u>3715-3603 BCE (69.5%)</u> 3588-3528 BCE (19.3%)
		C08	LTL21216	Org	4955 ± 45	3914-3876 BCE (5.8%) <u>3804-3641 BCE (89.6%)</u>

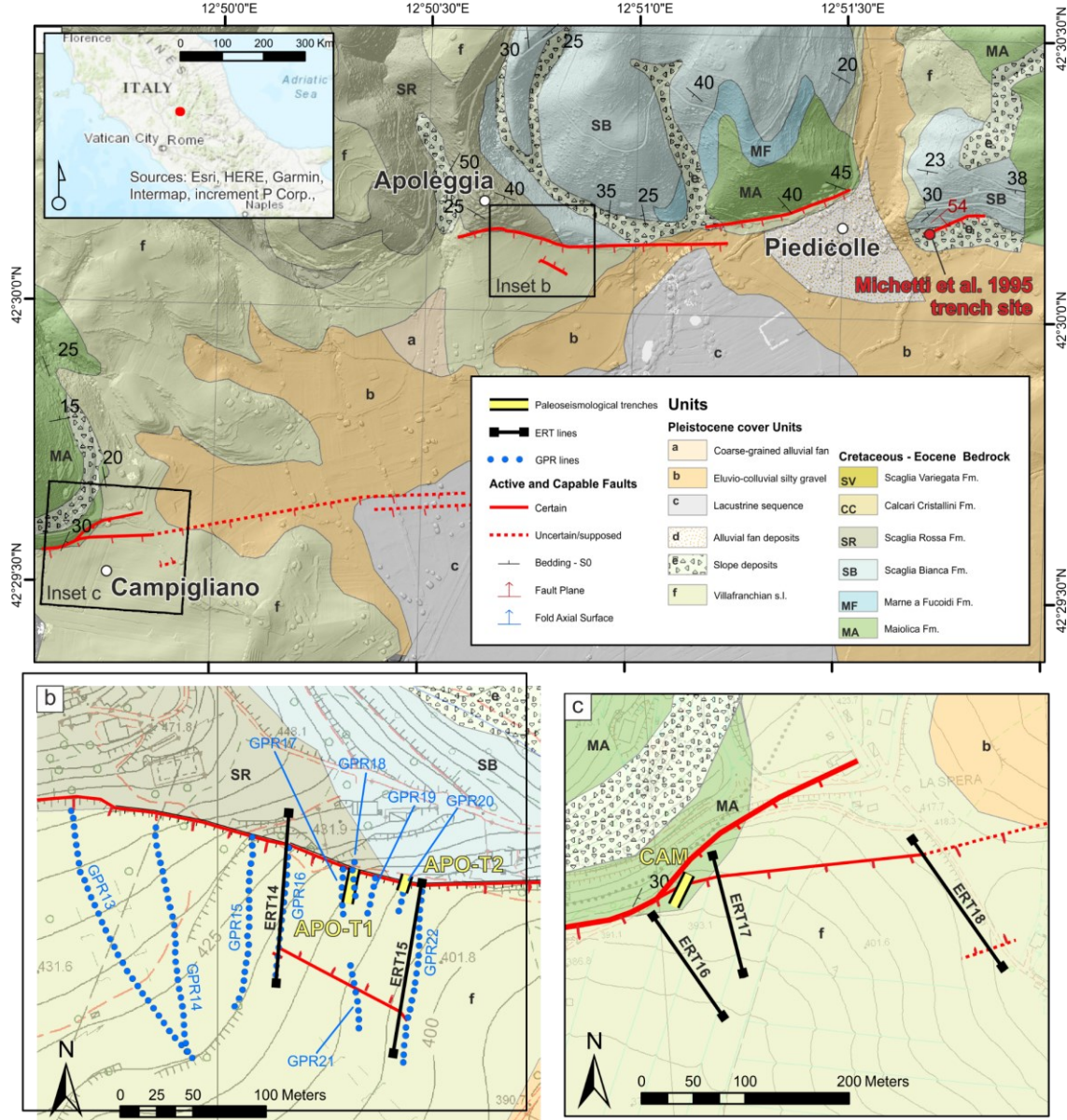
		C09	LTL21217	Org	4700 ± 45	3625-3560 BCE (17.3%) <u>3533-3370 BCE (78.1%)</u>
		C11	LTL21218	Plant remains	After 1950 CE	After 1950 CE
Rivodutri	CAM	C04	LTL22569	Org	15765 ± 120	17415-16872 BCE (95.4%)
		C06	LTL22570	Org	26571 ± 100	<u>29147-28749 BCE (87.0%)</u> 28666-28486 BCE (8.4%)
		C08	LTL22571	Org	17734 ± 65	19879-19280 BCE (95.4%)
		C10	LTL22572	Org	18557 ± 75	20739-20353 BCE (95.4%)
Cantalice	CUC	C02	Beta 634825	Charc	2280 ± 30	<u>401-351 BCE (51.3%)</u> 302-208 BCE (44.1%)
		C03	Beta 634826	Charc	2440 ± 30	<u>591-408 BCE (62.3%)</u> 751-684 BCE (22.3%) 668-634 BCE (9.7%) 622-613 BCE (1.1%)
	CANT-T1	C01	LTL21209	Charc	After 1950 CE	-
		C03	LTL21210	Charc	After 1950 CE	-
		C05	LTL21205	Charc	138 ± 40	<u>1797 - 1945 CE (57.3%)</u> 1670 - 1780 CE (38.1%)
	CANT-T3	C01	LTL22573	Org	17860 ± 65	20000 – 19475 BCE (95.4%)
		C02	LTL22574	Org	13860 ± 65	15083 – 14651 BCE (95.4%)
		C03	LTL22575	Org	9797 ± 45	9326 – 9206 BCE (95.4%)
Rieti	TR 1	C01	Beta 631859	Org	8710 ± 30	<u>7818-7597 BCE (94.6%)</u> 7931-7922 BCE (0.8%)
		C02	Beta 631860	Orgt	5000 ± 30	<u>3811-3701 BCE (65.2%)</u> 3942-3865 BCE (24.2%) 3682-3655 BCE (5.9%)
		C03	Beta 631861	Org	4310 ± 30	3011-2885 BCE (95.4%)

		C04	Beta 631856	Org	7510 ± 30	<u>6438–6340 BCE (71.9%)</u> 6313-6256 BCE (23.5%)
		C05	Beta 631857	Org	18670 ± 60	20919–20458 BCE (95.4%)
Rieti	TR 5	C03	Beta 631858	Org	4060 ± 30	<u>2673–2474 BCE (88.7%)</u> 2843-2813 BCE (6.3%) 2738-2735 BCE (0.4%)
Rieti	Villa Stoli South	C12	CEDAD LTL21261	Org	19127 ± 75	21261-20961 BCE (95.4%)
		C16	CEDAD LTL21260	Org	11801 ± 55	11835-11630 BCE (85.0%) 11601-11563 BCE (10.4%)
Santa Rufina (Cittaducale)	TR 3	C01	Beta 632175	Org	5270 ± 30	<u>4171-4036 BCE (60.9%)</u> 4233-4192 BCE (18.8%) 4027-3987 BCE (15.7%)
		C02	Beta 632176	Org	8640 ± 30	7729-7589 BCE (95.4%)
		C03	Beta 632177	Org	4870 ± 30	<u>3711-3627 BCE (87.7%)</u> 3560-3534 BCE (7.7%)
		C04	Beta 632178	Org	4550 ± 30	<u>3243-3102 BCE (57.2%)</u> 3371-3306 BCE (35.1%) 3300-3283 BCE (2.1%) 3276-3266 BCE (1.0%)
		C05	Beta 632179	Org	5910 ± 30	<u>4846-4712 BCE (95%)</u> 4878-4875 BCE (0.4%)
		C06	Beta 632180	Org	6000 ± 30	4988-4797 BCE (95.4%)
		C07	Beta 632181	Org	1690 ± 30	<u>326-424 CE (78.6%)</u> 255-286 CE (16.8%)
		C08	Beta63482 7	Char	8700 ± 30	7799-7597 BCE (95.4%)
Santa Rufina (Cittaducale)	TR 4	C01	Beta 632182	Org	1770 ± 30	224-376 CE (95.4%)
	CAS	C01*	GX-16336	Org	1530 ± 80	382-657 CE (95.4%)

Rivodutri, La Casetta		C02*	GX-16338	Org	1635 ± 85	245-594 CE (95.4%)
		C03*	GX-16335	Org	2865 ± 150	1436-786 BCE (95.4%)
		C04*	GX-16333	Org	3110 ± 90	1604-1583 BCE (0.8%) <u>1544-1116 BCE (94.7%)</u>
		C05*	GX-16330	Org	4055 ± 175	3089-3056 BCE (0.7%) <u>3034-2128 BCE (93.7%)</u> 2091-2042 BCE (1.1%)
		C06*	GX-16337	Org	5040 ± 100	4044-4012 BCE (2.4%) <u>3999-3640 BCE (93.0%)</u>
		C07*	GX-16332	Org	6425 ± 130	<u>5623-5205 BCE (89.4%)</u> 5173-5070 BCE (6.1%)
		C08*	GX-16331	Org	19800 ± 1650	26596-18541 BCE (95.4%)
		C09*	GX-16334	Org	20700 ± 1600	27370-19763 BCE (95.4%)
Rivodutri	PDC	C01*	GX-18926	Org	2265 ± 80	<u>541-95 BCE (94.6%)</u> 73-56 BCE (0.8%)
		C02*	GX-18925	Org	3440 ± 90	2008-2004 BCE (0.2%) <u>1971-1517 BCE (95.2%)</u>
		C03*	GX-18924	Org	5305 ± 150	4446-3794 BCE (95.4%)
		C04*	GX-18923	Org	6770 ± 215	6077-5307 BCE (95.4%)
		C05*	GX-18922	Org	10810 ± 470	11787-11764 BCE (0.2%) 11701-11686 BCE (0.1%) <u>11660-9322 BCE (95.1%)</u>
		C06*	GX-18921	Org	13490 ± 235	15056-13695 BCE (95.4%)
		C07*	GX-18920	Org	15650 ± 680	18814-15483 BCE (95.4%)
Cava Caporio	Caporio	C01*	GX-17913	Org	33300 +6400/-3500	
		C02*	GX-17916	Org	>37000	
		C03*	GX-17914	Org	>42000	
		C04*	GX-17915	Org	>37300	

4.1 Rivodutri area: Northern Border Fault

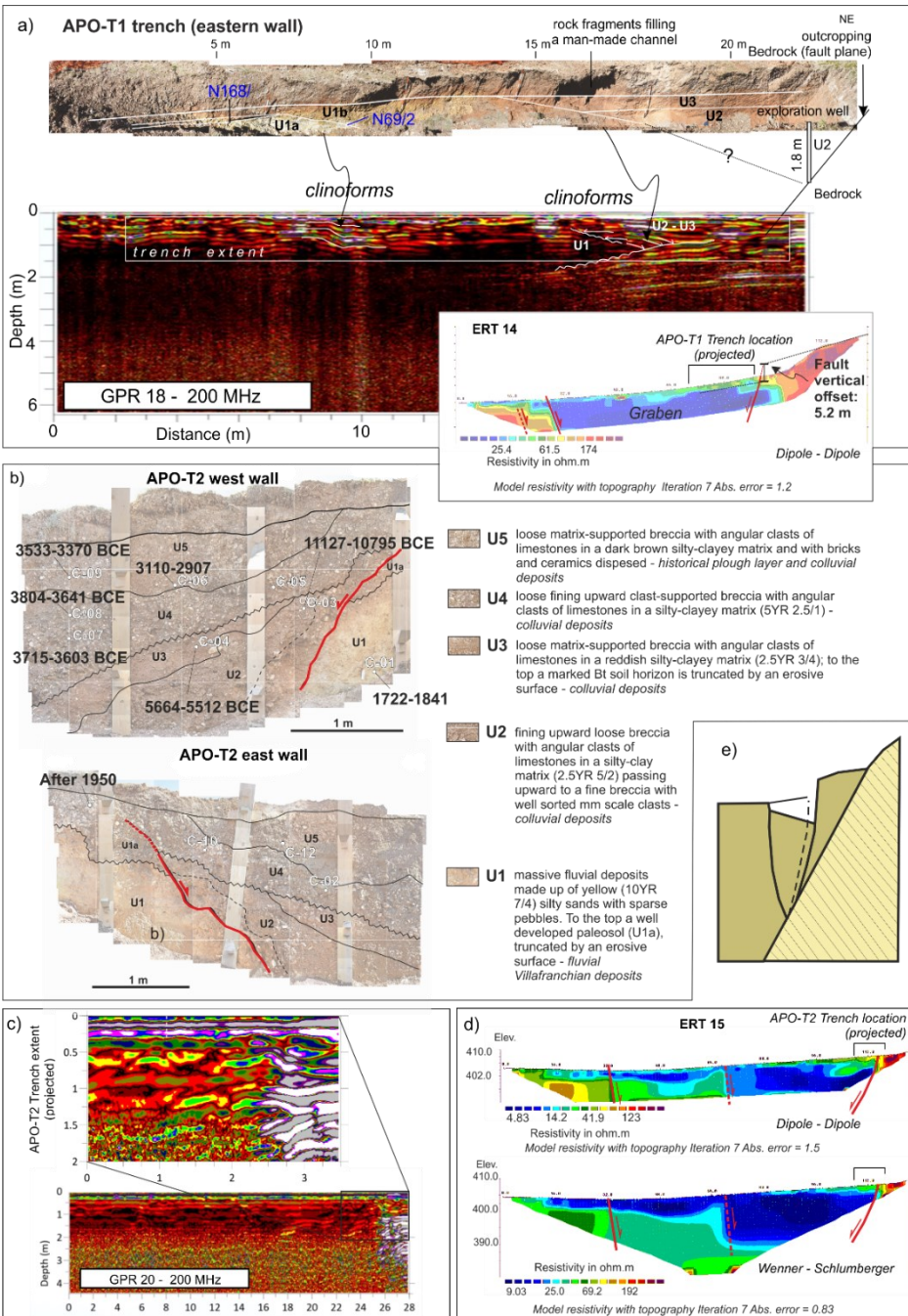
189 The northern Area includes two Sectors of investigation: Campiglano Sector, to the west and Piedicolle / Apoleggia Sector, to the east (Fig. 2a). We excavated 4 exploratory trenches in the Piedicolle / Apoleggia Sector, and one trench in the
 190 Campiglano Sector. In the following, we present results from two paleoseismological trenches at the Apoleggia Sector (APO-
 191 T1 and APO-T2; Fig. 2b) and one in the Campiglano Sector (CAM; Fig. 2c).
 192



194 **Figure 2: Study Area along the Northern Border fault: a) simplified geological map; b) and c) panels display detailed views on the**
 195 **196 two studied Sectors with the traces of the capable faults, of the geophysical investigations and the footprints of the excavated**
 paleoseismological trenches; red dot in Fig. 2a is the Piedicolle trench Site from Michetti et al. (1995)

197 The fault scarp we investigated at Apoleggia Sector shows all the characteristics of a typical post-glacial bedrock fault scarp
198 (Roberts and Michetti, 2004, and references therein). The topographic profile of the bedrock fault scarp at the Apoleggia Site
199 shows a minimum post-glacial vertical displacement of 5.2 m (Fig. 3). This value is calculated by projecting the topographic
200 slope in the footwall below the thickness of historical slope deposits. In fact, ERT profiles clearly show the position of the top
201 of the Pleistocene lacustrine deposits, which is parallel to the footwall slope and can be regarded as a proxy for the glacial
202 topographic slope. As discussed in the literature, we assume that this vertical displacement occurred during the last 18 kyr and
203 we derive a consistent post-glacial slip-rate of 0.29 mm/yr at this site. We excavated two trenches at the contact between the
204 Cretaceous-Eocene Scaglia Rossa Fm. and the Early Pleistocene Villafranchian lacustrine deposits. Trench APO-T1 was 24
205 m long with a maximum depth of 3 m. We fully covered the excavation walls with detailed photographic survey. However,
206 due to problems in maintaining the stability of the trench walls, we could not prepare a grid for logging. The NE limit of the
207 trench is located a few meters from the bordering fault scarp characterized by the bedrock outcrop. We recognized four
208 stratigraphic units in the APO-T1 trench, reported on the log of Fig. 3a. The stratigraphic units are briefly described as follows:
209 U1a is comprised of white and light gray clays with calcium carbonate concretions at the base; U1b is a reddish-brownish soil
210 truncated at the top by an erosive surface; U2 is slope debris with angular flint; U3 is a colluvial deposit characterized by
211 loose limestone breccia with angular flint and minor calcareous clasts; U4 is a colluvial deposit characterized by loose
212 limestone breccia with prevalent calcareous clasts and probably very recent brick fragments. APO-T1 shows a man-made hole
213 filled with limestone blocks of various sizes between 15 m and 20 m (each trench is labelled with progressive numbers in
214 meters from the beginning of the excavation; Fig. 3a). An exploratory well was drilled with a hand auger in the NE end of the
215 trench. The drilling crossed the loose limestone breccia of Unit 2 until it touched the limestone bedrock at a depth of 1.8 m
216 below the bottom of the trench (Fig. 3a), thus constraining the geometry of the fault scarp at depth. Furthermore, APO-T1
217 shows some clinoforms possibly related to a rollover anticline whose geometry is consistent with that of the bordering fault
218 (Figure 3a). The clinoforms are also visible in the GPR_18 (Figure 3a) located at the same position of APO-T1 (Fig. 2b).
219 Figure 3 shows the ERT_14 section (see location in Fig. 2b); the main fault, dipping towards the S, separates a sector with
220 resistivity greater than 150 Ω m in the footwall, with a sector of low resistivity in the hanging wall (5-20 Ω m). The ERT_14
221 profile shows another clear change in the resistivity values, which can be associated with an antithetic fault dipping toward the
222 N. Similar results are obtained from the ERT 15, presented in Figure 3d in dipole-dipole configuration, above, and Wenner-
223 Schlumberger, below.
224 The trench APO-T2 uncovered a sedimentary sequence comprising 5 units that were displaced along normal fault planes. The
225 stratigraphic units are described as follows: U1 is a massive fluvial deposit with yellow (10YR 7/4) silty sands; U2, U3, U4
226 and U5 are colluvial deposits characterized by a loose calcareous breccia with angular clasts in a silty-clay matrix with different
227 colors from reddish brown, in U2, to dark brown, in U5. Figure 3c shows the interpreted trench stratigraphy photomosaic and
228 the paleoseismic history reconstructed at the Site. The trench crossed a typical earthquake gravity graben (*sensu* Gilbert, 1897;
229 Slemmons, 1957; Fig. 3e). The main fault plane outcrops a few meters outside the trench, whereas in the trench, a secondary
230 fault shows evidence of repeated movements that occurred during the deposition of Units 2-5. An older earthquake is inferred

231 from the deformation of Units 2 and 3: the top of Unit 2 and some stratigraphic markers within the unit are deformed and
232 inclined by the fault plane. We interpret Unit 3 as a fine-grained colluvial wedge that was deposited after the first earthquake;
233 this paleoseismic event is chronologically constrained by 14C dates between 11127 and 5512 cal yr BCE, with a minimum
234 offset of 15 cm. A second paleoearthquake is identified from the deformation of Units 3-5. The top of U5 is undeformed, and
235 the minimum offset of the underlying units is 22 cm; the age of this earthquake is between 3533 and 2907 cal yr BCE.
236 We excavated CAM trench (see location in Fig. 2c) for a length of 22 m and a maximum depth of 3 m. The stratigraphic units
237 recognized are on the CAM trench log of Figure 4a. The sedimentary sequence exposed in the CAM trench (Fig. 4a) has silts
238 and clays of the Villafranchian series (U1) at its base, presumably related to the Monteleone Sabino Unit (refer to Cavinato
239 1993 for the basic reference about the local Plio-Quaternary Stratigraphic units). An erosive surface truncates this unit at the
240 top. Loose sands and silts, with lenses of coarse gravel fining upwards to compacted silty clays (U2), lie on top of U1. This
241 unit is interpreted as a colluvial depositional environment.
242 The succession is closed, at the top, by colluvial reddish silty sands (U3). The beds of the units and their lower and upper limits
243 are crosscut by a series of faults that also induced considerable folds and deformation within the sediments. Three fault strands,
244 belonging to the same deformation zone, have been identified and coded as Fault A, B and C in Figure 4a. The main fault
245 strand is in fact located outside the trench, at an outcrop along a road cut that prohibited direct trenching. At this road cut
246 location, the Villafranchian conglomerates of the Fosso Canalicchio Unit outcrop along a bedrock fault scarp that puts the
247 conglomerates in tectonic contact with recent colluvial sediments. Logistical limitations did not allow the main fault plane to
248 be directly investigated through a paleoseismological excavation; however, the trench wall exposed a series of subsidiary
249 structures. The main fault plane, in fact, outcrops ca. 30 m west of the trench limit and, projected towards the trench, it runs
250 only a few m to N of the trench. The fault plane dips towards the SE (Fig. 4a) and separates two different units within the
251 Villafranchian lacustrine series (Monteleone Sabino Unit). Two fault strands, synthetic to the main one (i.e., Fault A and C),
252 progressively displaced the hanging wall block. An antithetic fault (Fault B), slightly oblique to Fault A, delimits a graben that
253 widens toward the east. Overall, the 'Villafranchian' series in the hanging wall of the fault is downthrown and backtilted
254 northward, that is toward the main fault plane, forming an asymmetric half-graben (earthquake gravity graben sensu Gilbert
255 1897; Slemmons, 1957; Fig. 4c). Faults A and B displaced the top of U1 in all the walls of the trench. The top of U2 along the
256 east wall apparently seals both, while Fault A clearly displaces the same horizon in the west wall, with a cumulative vertical
257 offset of ca. 35 cm. Given the clay-rich lithology, the limited cumulative vertical offset (i.e., less than 10 cm on a single fault
258 strand) and the gradual transitions between units, we believe that both faults can be considered active during the deposition of
259 the U3 colluvial deposit, and that U2 recorded the ultimate movement younger than 17415-16872 BCE. Fault C, synthetic to
260 the main one but with low-angle bedding, appears to be sealed by U2 along the east wall, while displacing the base of U3 at
261 the west wall. The total vertical offset of Fault C, measured at some levels in the Villafranchian deposits, is ca. 113 cm, while
262 the base of U3 appears to be displaced by only 27 cm. In this case, Fault 3 is also considered to have been reactivated with the
263 last movement during the deposition of U3.

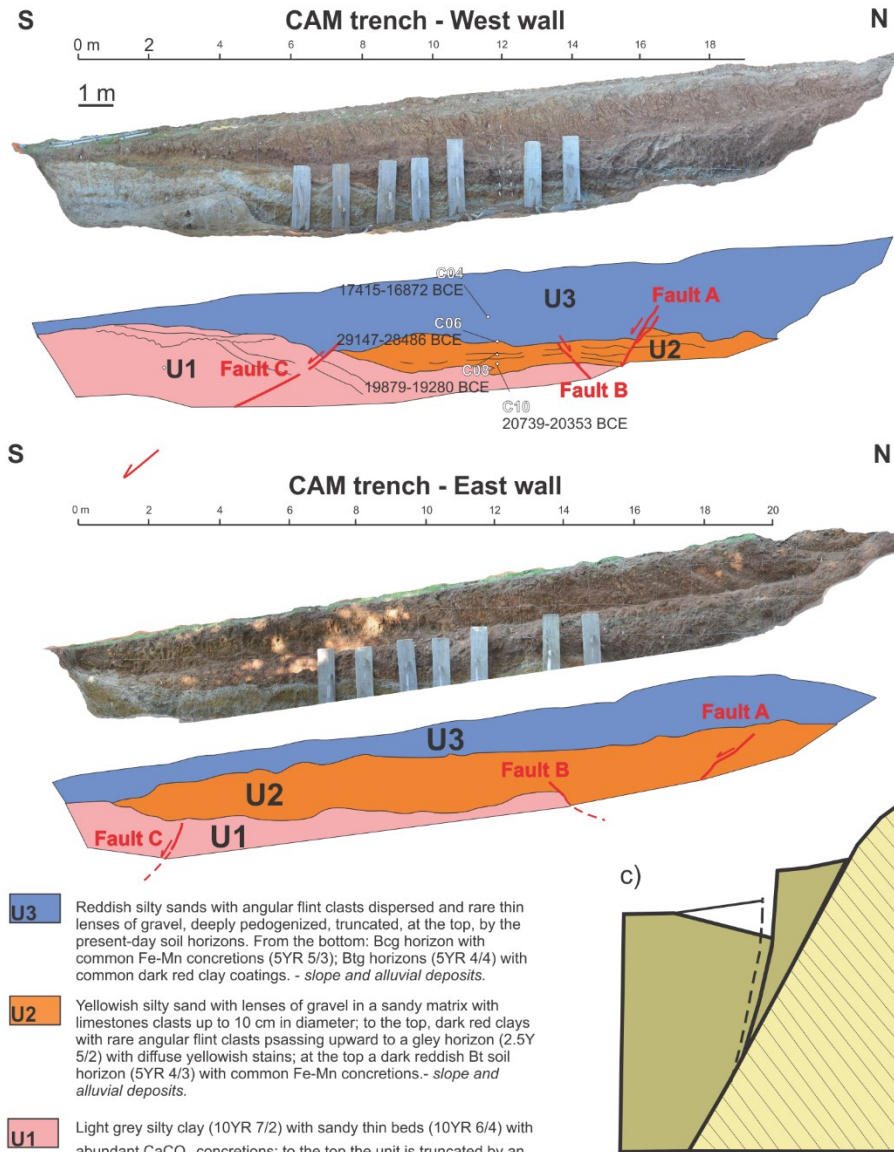


266
267
268
269
270

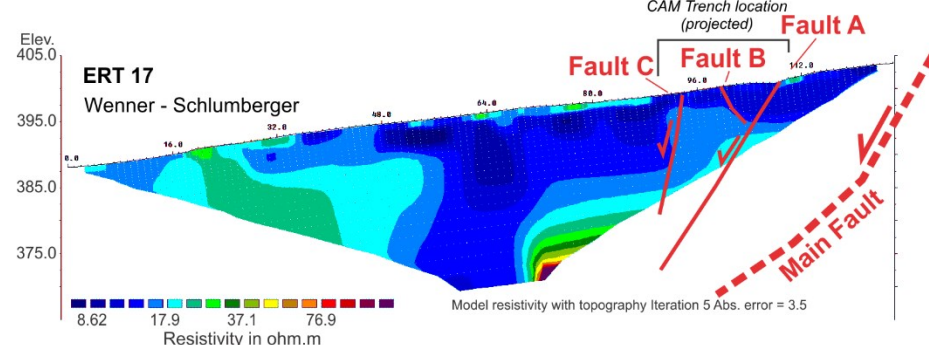
Figure 3: Paleoseismological trench and investigations along the Northern Border fault – Apoleggia Sector (see Figure 2 for the locations of trenches and geophysical line traces): a) APO-T1 trench eastern wall (for details on the cal ages see Table 1) and comparison with the GPR 18 and ERT14 lines; b) APO-T2 trench walls; c) GPR20 line; the inset shows a focus on the footprint of the APO-T2 trench (projected); d) ERT15 lines with indicated the footprint (projected) of the APO-T2 trench; (e) model of the gravity graben following the Gilbert's theory of grouped fault scarps in alluvium (redrawn after Gilbert, 1890; Slemmons, 1957).

271 CAM_ERT_17 section in Figure 4b appears to show a slight discontinuity in the resistivity values in its northern sector, along
272 the progressive 90 and 70 m, probably associated with a S dipping fault. The high resistivity values at the base of the section,
273 along the progressive 70 m, may be associated with the bedrock. It is worth noting that the section does not reach the bedrock
274 at surface: the fault plane on bedrock is ca. 30 m far from the northern end of the section. Furthermore, a vertical change in the
275 resistivity values along the progressives 32-45 m may be associated with an antithetic fault dipping towards the N.

a)



b)

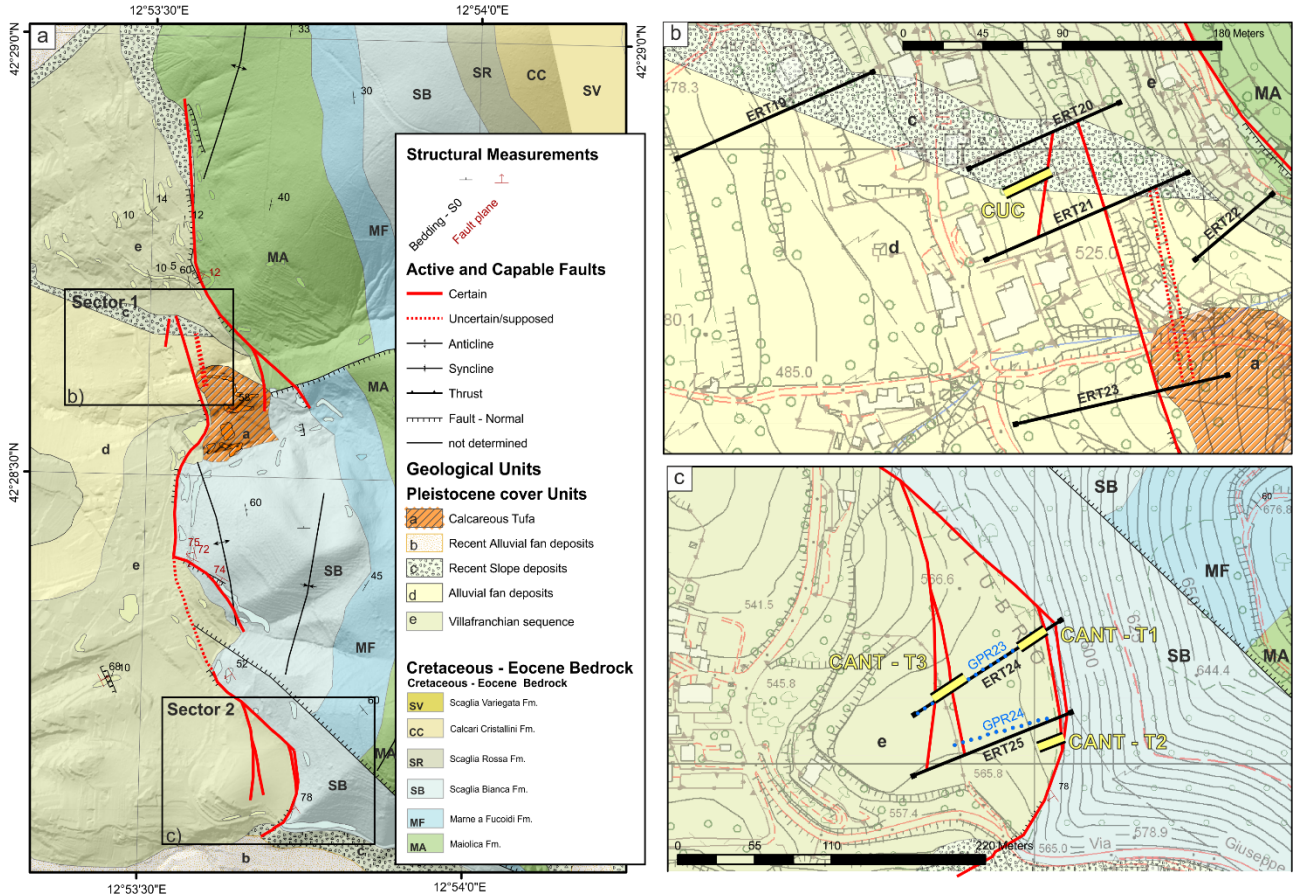


277 **Figure 4: Paleoseismological trench and investigations along the Northern Border fault, Campiglano Sector; CAM trench (see**
 278 **Figure 2 for trench location); (a) photomosaic of the western and eastern walls (for details on the calibrated ages see Table 1); (b)**
 279 **Wenner -Schlumberger ERT 17 line (trace in Figure 2), the location of the CAM trench (projected) is indicated; (c) model of the**
 280 **gravity graben following the Gilbert's theory of grouped fault scarps in alluvium (redrawn after Gilbert, 1890; Slemmons, 1957).**

281 4.2 Cantalice area: Eastern Border Fault

282 We investigated the Eastern Border fault at two Sectors along the same fault strand (Fig. 5a). We excavated one trench in
 283 Sector 1 (Fig. 5b) and three trenches in Sector 2 (Fig. 5c), two of which will be presented in the following section. For the
 284 whole dataset, please refer to the Supplementary Material.

285



286 **Figure 5: Study Area along the Eastern Border fault: a) simplified geological map; b) and c) panels display detailed views on smaller**
 287 **sectors with the mapped capable faults, the traces of the geophysical investigations and the footprints of the excavated**
 288 **paleoseismological trenches.**

289 In Sector 1, we excavated the CUC trench for a length of 14 m and a maximum depth of 3 m. We reconstructed a stratigraphic
 290 sequence composed of four units, as described below, from the top to the base of the sequence. The uppermost unit of the
 291 stratigraphic sequence (U4) is represented by a matrix-supported conglomerate with well-rounded clasts of limestone (average
 292

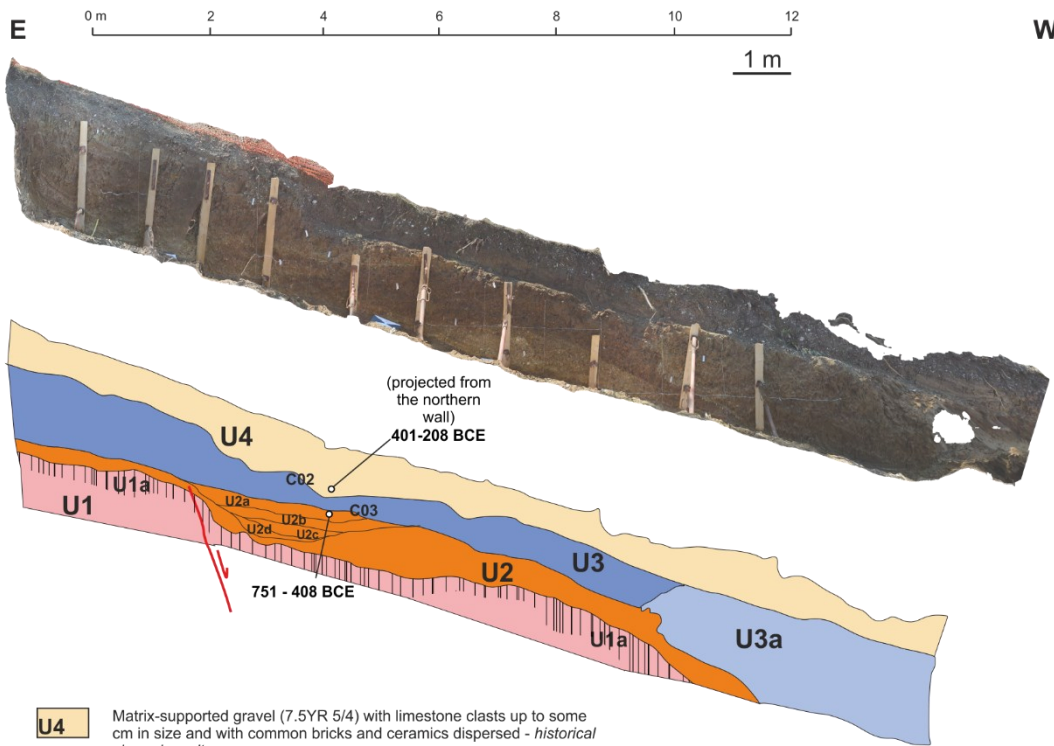
293 diameter 0.5 cm) embedded within a clay-rich matrix (7.5YR 5/4). Remains of roots, bricks and enameled ceramics are
294 dispersed within the matrix.

295 Unit U3 consists of a matrix-supported gravel made of carbonate clasts embedded within a clay-rich matrix. The matrix of the
296 U3 shows remarkable color variation, from 10YR 5/4; 10YR 4/3 up; 2.5YR 6/6 to base. At the top of the U3, the clasts show
297 frequent Fe (7,5YR 6/8) and Fe-Mn (10YR 3/2) coatings. The amount of Fe-Mn clast coating increases downward. The sub-
298 unit U3a shows local concentration of organic matter and Mn coatings (5YR 2.5/1) are present on clasts.

299
300 The unit U2 is made by a highly variable colored clay matrix (10YR 4/4; 10YR 3/1; 10yr 8/2) with rare limestone clasts
301 dispersed within it. The clasts show a maximum size of 3-5 cm, with evidence of partial reworking. In the central part of the
302 trench (i.e. progressive 2-4 meters; Fig. 6a) U2 has been split in several sub-units. From the base: the unit U2d consists of clay-
303 sandy matrix (7.5YR 4/3) with Fe-Mn (7,5YR 5/1) and Fe (7,5YR 5/8) coatings on limestone clasts. Some clasts of the U2d
304 unit are completely decarbonated. Above, the unit U2c is made of sandy-clay (10YR 4/4) with Fe-Mn levels of concretions
305 (7.5 YR 4/1). Unit U2b is made of a clay matrix (10YR 3/2) with millimeter clasts of limestones and flints. Clasts are covered
306 with Fe-Mn coatings (10YR 3/1). Finally, the unit U2a is made of a matrix-supported gravel of angular 1 cm sized clasts of
307 limestones and flint, dispersed in clay-rich sand (10YR 4/3). Clasts are locally covered with Fe (10YR 8/6) staining.

a)

CUC trench - South wall



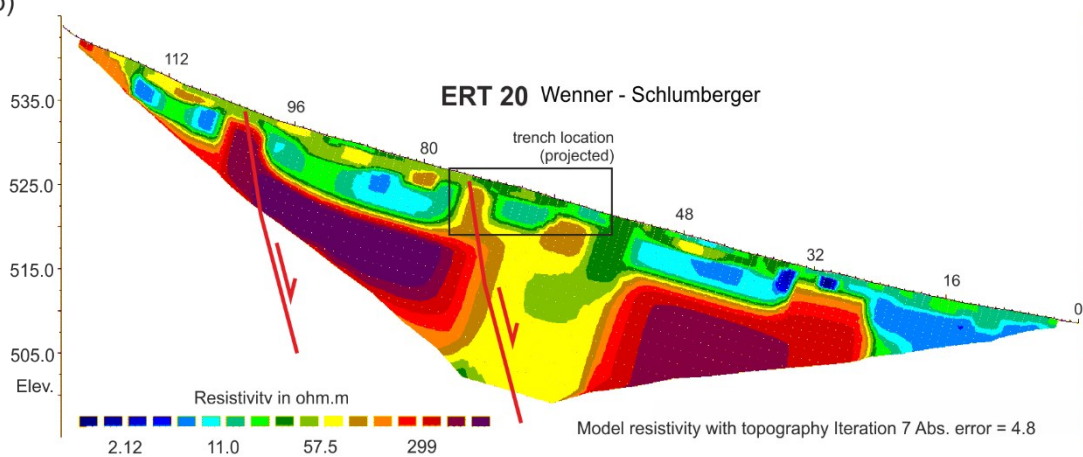
U4 Matrix-supported gravel (7.5YR 5/4) with limestone clasts up to some cm in size and with common bricks and ceramics dispersed - *historical slope deposits*.

U3 a Sandy clay with rare limestone and flint clasts up to 1 cm in size; frequency Fe-Mn concretions and clay coatings, more common downward; downslope the unit is cut by and erosive surface and is laterally passing to a later unit (U3a) made up of light grey sandy clay with rare limestone clasts and common blocks of older soils reworked into the unit.

U2 Fining upward matrix-supported gravel in a clayey-silty matrix (10YR 4/4) with limestone clasts and common flints; close to the fault the units is organized into four wedge shaped lenses of fining-upward cycles of deposition; Fe-Mn concretions are common - *slope deposits and colluvial wedges*.

U1 Matrix supported calcareous sandy gravel, light brown, passing upward to a well-developed weathered horizon with frequent zombie stones and flint clasts (7.5YR 5/8); to the top, the unit is truncated by an erosive surface. - *Villafranchian sequence*.

b)



309 **Figure 6: Paleoseismological trench and investigations at the Sector 1 of the Eastern Border Fault: a) CUC trench, no vertical**
310 **exaggeration (southern wall; the footprint in Figure 5b; for details on the cal age determinations see Table 1); b) Wenner -**
311 **Schlumberger ERT survey (see trace in Figure 5b), the location of the CUC trench (projected) is indicated**

312 The lowermost unit (U1) is a considerably older sequence, represented by a clast-supported breccia. At its top, unit U1 shows
313 a decimeter-thick distinctive weathering horizon (U1a). The clasts inside the weathered horizon U1a are completely
314 decarbonated. At the top, this horizon is cut by an erosive surface (Villanfranchiano Auct.; Upper Pliocene – Lower
315 Pleistocene). A normal fault, dipping towards W, offsets the sequence exposed at the CUC trench, down-throwing the lowest
316 stratigraphic units of the sequence, i.e., U1-U2. In the hanging wall of the fault, a wedge-shaped colluvial unit crops out (i.e.,
317 U2a – d). The fault exposed within the CUC trench shows a polyphasic activity, we observed that a cumulative offset of 87
318 cm is related to two surface rupturing events. The penultimate event shows an offset of 53 cm, while the last one shows an
319 offset of 34 cm. Both seismic events predate the deposition of the stratigraphic unit U3.

320 The calibrated dating results obtained from the samples of the CUC trench constrain the last activity of this fault within the
321 VI-V century BCE. In fact, the date of 751-408 BCE refers to the wash facies of the upper colluvial wedge (Unit U2a), which
322 postdates the last surface faulting event. We remark that also the dated sample from Unit 4 gives a similar calibrated age of
323 401-208 BCE; the whole sequence of slope deposits therefore formed in a few centuries after the observed surface faulting
324 events. It is possible to hypothesize that the fault splay located upslope from the trench that was imaged in the ERT 20 profile
325 (Fig. 6b) also slipped during the same events. The 53 cm offset observed during the penultimate event in the CUC trench, that
326 is relatively large when compared with the other trenches excavated during our investigations, might nevertheless be a
327 minimum value for the coseismic displacement at this site. This would seem to agree with the position of the CUC trench
328 located along the main fault of the Rieti Basin, where we expect the highest displacement during a strong earthquake.

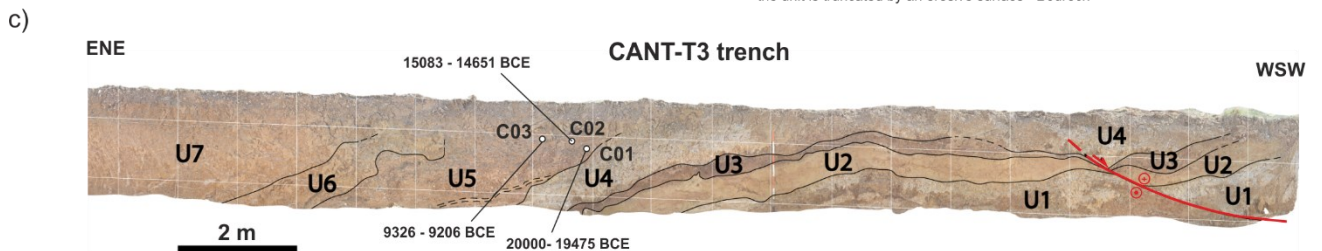
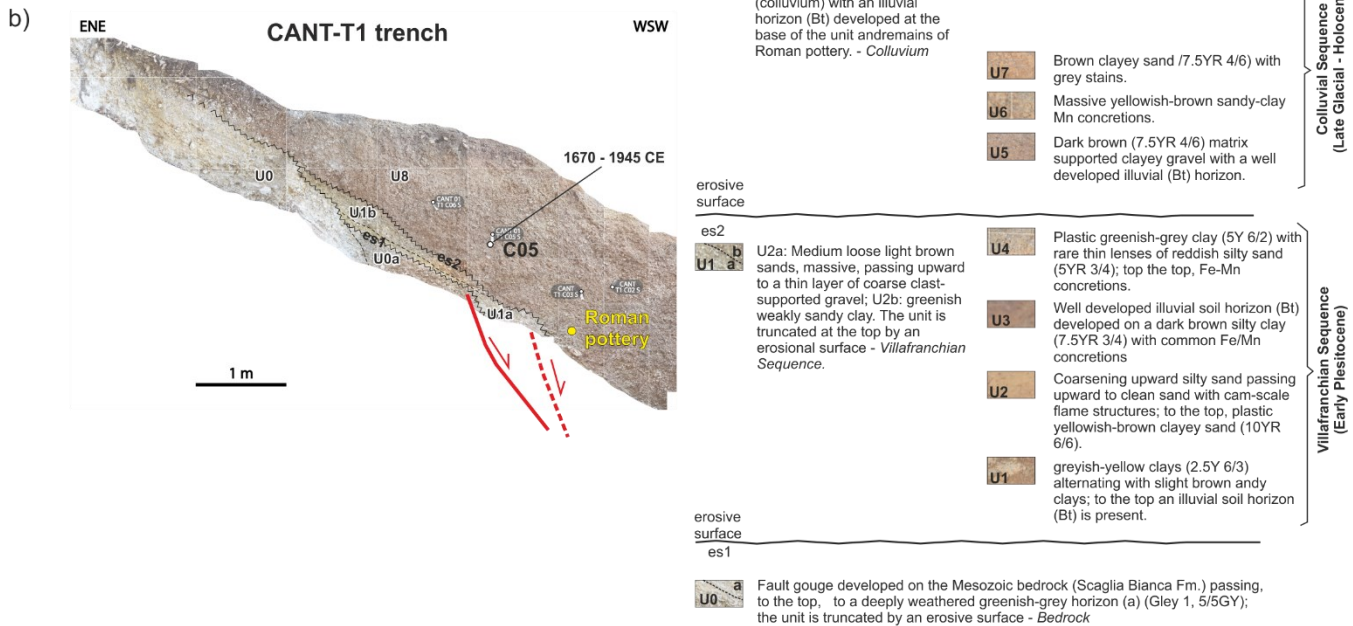
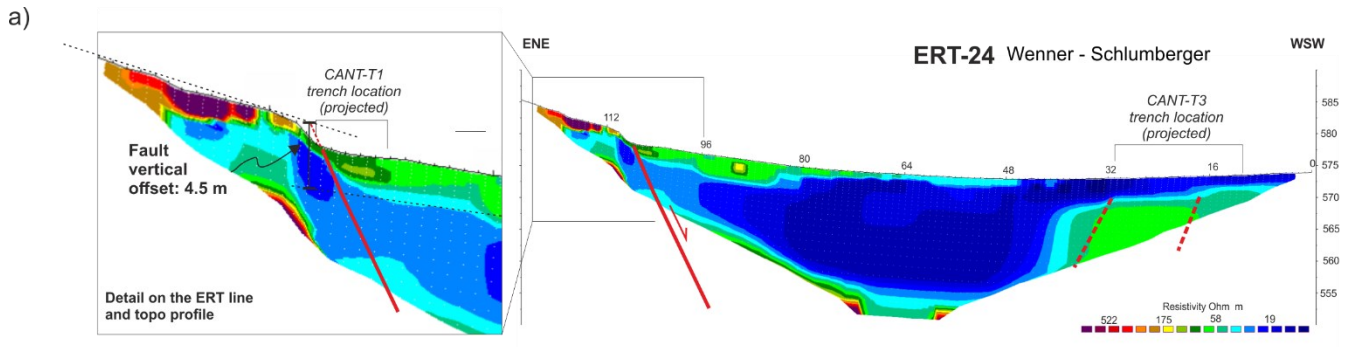
329 At Sector 2, we investigated a strand of the eastern border fault, where a well-expressed bedrock fault scarp in the Cretaceous
330 Scaglia Bianca Fm. faces a nearly flat paleosurface. The fault scarp we investigated shows all the characters of a typical post-
331 glacial limestone fault scarp (Roberts and Michetti, 2004, and references therein). We acquired two ERT lines (24 and 25; Fig.
332 5c) that clearly show the tectonic contact between the high resistivity limestone and a package of conductive slope deposits at
333 least 15-20 m thick. To the WSW, the ERT 24 line shows two other abrupt steps in the resistivity units, consistent with a set
334 of antithetic normal faults, bounding the flat paleosurface. Topographic profiles of the bedrock scarp and thickness of Late
335 Holocene to historical slope deposits show a minimum post-glacial vertical offset of 4.5 m (Fig. 7a), hence a slip-rate of 0.25
336 mm/yr.

337 The lateral contact between the ERT units, at the ENE tip of the ERT line, well fits with the location of the morphological
338 scarp at the contact between the Cretaceous Scaglia Bianca Fm. and the Villafranchian lacustrine deposits, and with the
339 occurrence of a fault plane, that has been exposed by trench excavation (trench CANT-T1; Fig. 7b). CANT-T1 trench exposes
340 a sequence of Pleistocene Villafranchian units (U1 in Fig. 7b) separated by erosive surfaces, lying directly on a deeply
341 weathered bedrock (U0). The Villafranchian, in turn, is covered by a thick bed of massive colluvial deposits of Late Glacial to
342 historical age (U5). At the contact between the bedrock and the U1 unit an abrupt step was exposed, marked by the fold and

343 lowering of U1 toward the hanging wall block. A discrete fault plane has not been observed here, and we were not able to
344 excavate further in the trench for security reasons. The fault zone is here expressed as a wide and distributed zone of strain
345 accommodation, due to the highly plastic weathered units exposed. Nonetheless, episodic deformation events are here
346 confirmed by the geometry of the erosive surfaces, with the erosive surface “es1” being deformed by a first fault movement,
347 predating the erosive surface “es2”, instead. A possible second fault movement, can be inferred based on the abrupt step, only
348 partially exposed, that the “es2” displays just on the floor of the trench.

349 Trench CANT-T3 exposes a sequence of Villafranchian units (U1 to U4; Fig. 7c), overlain by a sequence of colluvial beds
350 with intercalated paleosol horizons. The units are involved in a set of asymmetric folds, which we interpret to be related to
351 underlying blind normal faulting, based on the features of the ERT-24 line described above. Dated samples in the colluvial
352 units indicate a Late Glacial to Holocene age. The colluvial beds, steeply dipping toward the mountain front, constitute the
353 syn-growth sedimentation of the graben-structure with a contemporary infilling of the subsiding block. To the WSW, the trench
354 also exposes a secondary normal fault in the Villafranchian Sequence, dipping to the SSE, crosscut almost along strike by our
355 trench, and testifying to complex deformation and hanging wall release faulting in the graben block.

356 From the features described above, we can constrain several fault movements for this fault strand since Late Pleistocene.
357 Deformation is distributed into a wide deformation zone with the development of a graben structure and near-surface fault-
358 related extensional folds.



360 **Figure 7: Paleoseismological trench and investigations at the Sector 2 of the Eastern Border Fault: a) ERT line with a zoom in on**
 361 **the fault scarp (see trace in Figure 5c); b) and c), paleoseismological trenches T1 and T3 respectively (the trenches footprints in**
 362 **Figure 5c; for details on the cal ages see Table 1).**

363 4.3 Rieti – Santa Rufina area: Southern Border Fault

364 The third Study Area extends about 5.5 km east of the historical center of Rieti, up to Santa Rufina, a hamlet of Cittaducale
 365 (RI), along the eastern part of the Rieti Southern Border Fault. The southern Area includes three Sectors of investigation (Fig.

366 8). We dug seven exploratory trenches in this Area (Figure 8b-d). Below, we describe the results of paleoseismological
367 investigations carried out only on the three trenches (TR1, Villa Stoli South and TR3) where we find primary coseismic
368 elements and, as examples of the structural styles of the fault zone, we show two trenches with only secondary elements (TR4
369 and TR5; Figure 8).

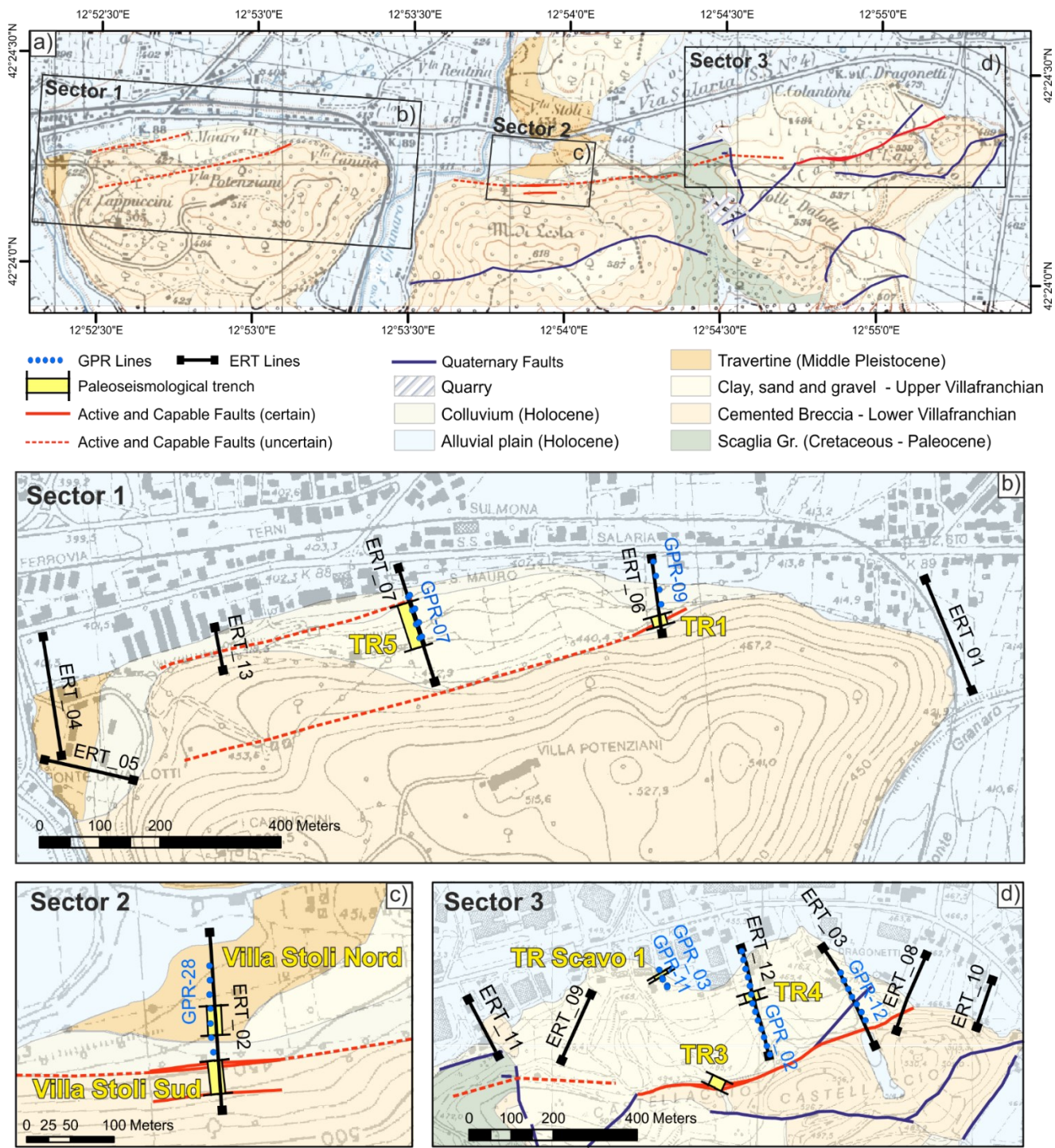


Figure 8: Study Area along the Southern Border Fault: a) simplified geological map; b), c) and d): detailed views on the three studies Sectors (extent is shown in a) with boxes) with the traces of the capable faults and of the geophysical investigations and the footprint of the excavated paleoseismological trenches.

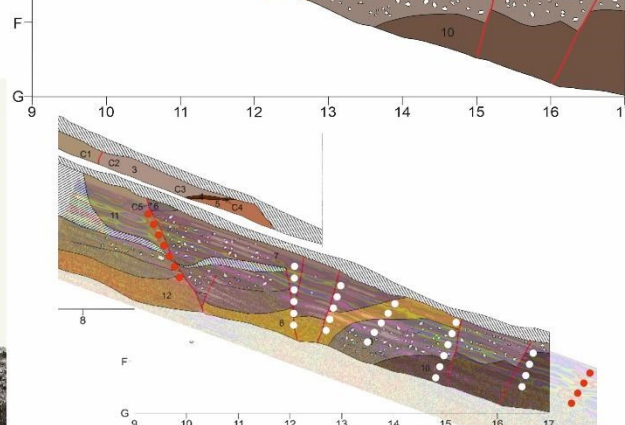
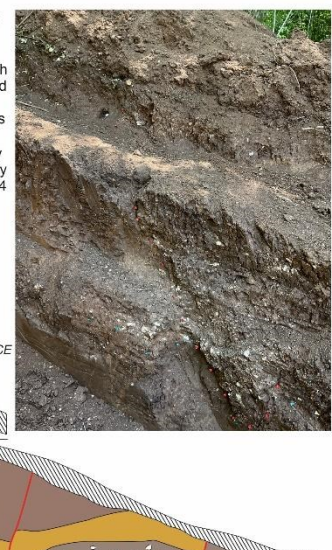
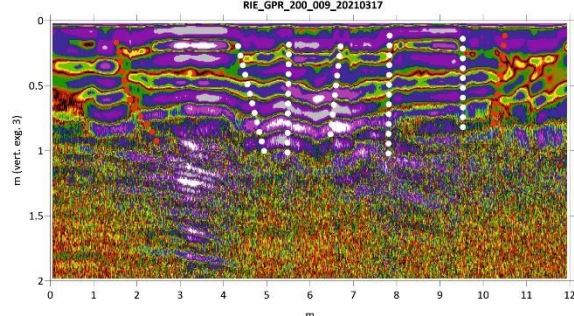
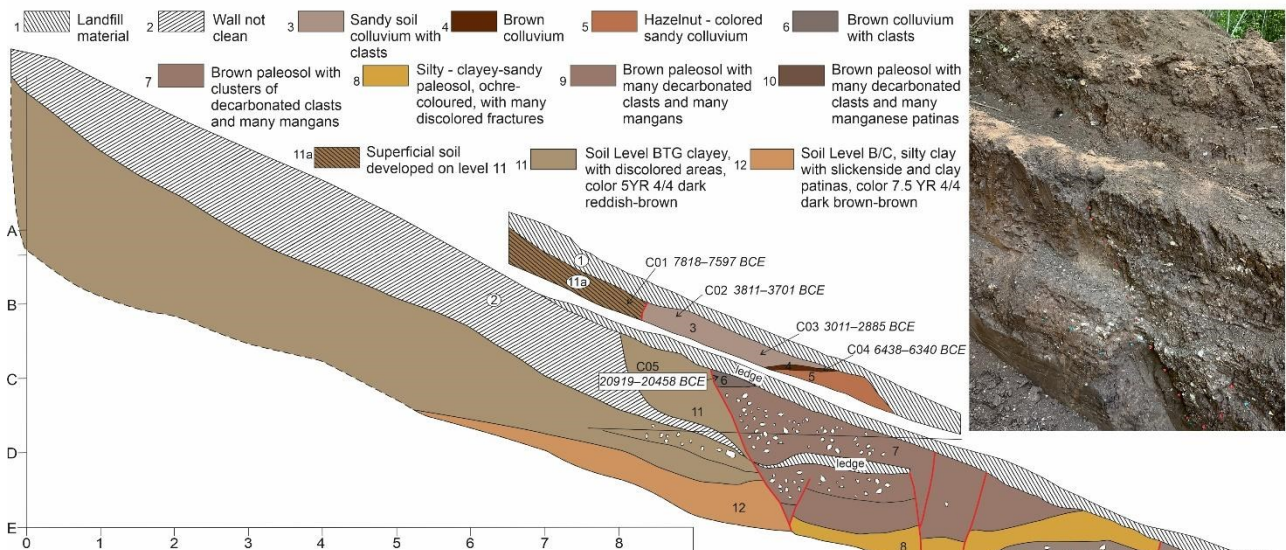
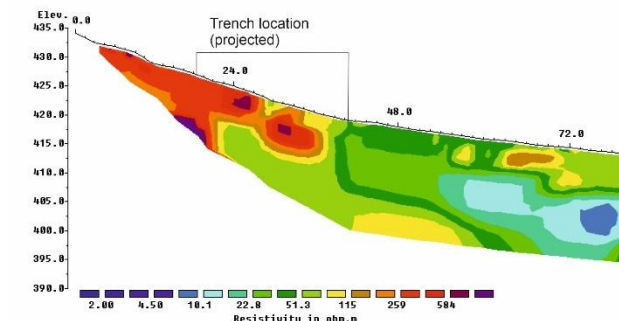
374 **4.3.1 Sector 1: Trenches TR1 and TR5**

375 The 20 m long trench TR1 was excavated (location in Fig. 8b) with a NW-SE orientation where ERT 06 and GPR Line 09
376 investigations showed clear geophysical discontinuities. Figure 9 shows the result of the inversion of the Dipole-Dipole data
377 acquired along the ERT 06 profile (RMS 9.4%, 4 iterations) using 72 electrodes with an equidistance of 3 m. The tomographic
378 model shows, in its southernmost part, two significant lateral variations in resistivity. In the same zone, also the GPR 09 profile
379 shows several discontinuities in the electromagnetic characteristics of the shallow part of the terrain (dots lines). TR1
380 confirmed the occurrence of a fault zone affecting both the Monteleone Sabino Synthem (Early Pleistocene, Upper
381 Villafranchian in Fig. 8), which in this sector is completely pedogenised, and the recent *colluvia* above, outcropping in the
382 upper wall of the excavation. As shown in Figure 9, the trench wall has in fact a ca. 1.5 m thick lower part, separated from the
383 upper ca 70 cm thick upper part by a step about 1 m wide (“ledge” in Fig. 9).

384 The overlap between the stratigraphic log and the corresponding section of the GPR 09 profile clearly illustrates how the
385 discontinuities detected by the radar correspond well to those observed in the trench. This result confirms the effectiveness of
386 GPR prospecting in the siting of paleoseismic trenches.

1-S

ERT 6 DD



387

388 **Figure 9: Southern Border Fault, Sector 1, trench log and geophysical profiles at Trench 1 Site; Above: ERT 6 and Gpr 09 profiles;**
 389 **Below: Stratigraphic log of the W wall of trench 1, accompanied by a legend describing the various pedogenized deposits of the**
 390 **Monteleone Sabino Synthem and the overlying *colluvia* in clear discordance; the photomosaic of the lower west trench wall**
 391 **(progressive 7 m to 17 m) is also shown together with a detail of the major fault localized between progressive 8 and 11m; on the**
 392 **bottom right, the overlap of the stratigraphic log and the GPR profile.**

393 Figure 9 also presents the stratigraphic log of the W trench wall, accompanied by a legend that describes the various colluvial
394 and soil horizons. Please refer to this legend for details on the stratigraphy visible in the trench walls. Throughout the trench,
395 an ancient and deep pedogenesis characterizes Unit 11. However, in the upper part of the trench Unit 11 is affected by a much
396 more superficial and recent soil horizon (Unit 11a), dated at 7818-7597 BCE. A N60°E trending, 70° NW dipping, fault offsets
397 the Monteleone Sabino Synthem, such that the soil horizons present at its footwall do not correlate with any of the horizons at
398 its hanging wall; the same fault also displaces the overlying succession of colluvial deposits. We identified this fault as the
399 major fault at the base of the northern slope of the Cappuccini-Villa Potenziani relief.

400 In the upper wall of the trench, this fault brings in contact the pedogenized Monteleone Sabino Synthem, here characterized
401 by a recent superficial soil horizon (indicated as Unit 11a), with a soil colluvium (Unit 3). The calibrated age of the faulted
402 units provided age ranges of 7818–7597 BCE (Sample C01, Table 1) and 3811 –3701 BCE (Sample C02), respectively. This
403 means that a surface faulting event occurred after 3811-3701 BCE (event TR1-2 in Fig. 15).

404 In the lower wall of the trench, the fault brings Unit 11 in contact with a colluvium (Unit 6) which, due to its geometry, we
405 interpret as a colluvial wedge. This colluvial wedge returned a calibrated age of 20919–20458 BCE (Sample C05) and,
406 considering its thickness, it is possible to estimate a surface dislocation of at least 15 cm necessary for it to be deposited. This
407 event occurred just before the deposition of the colluvial wedge, then before 20919–20458 BCE (event TR1-1 in Fig. 15).

408 In sector 1 (Fig. 8b) we also excavated the trench TR5, providing evidence of several tectonic dislocations of the Monteleone
409 Sabino Synthem deposits (Fig. 10). We interpreted these structures as secondary faults, presumably linked to a main fault
410 located just to the north. However, it was impossible to verify this hypothesis; we were not able to extend the exploratory
411 trench further N, due to the presence of an aqueduct.



412

413 **Figure 10: Southern Border Fault, Sector 1, trench 5 showed the Monteleone Sabino deposits dislocated by a dense grid of faults;**
 414 **the figure shows a portion of the east wall of the 77 m long trench, no vertical exaggeration.**

415 **4.3.2 Sector 2: Villa Stoli South Trench**

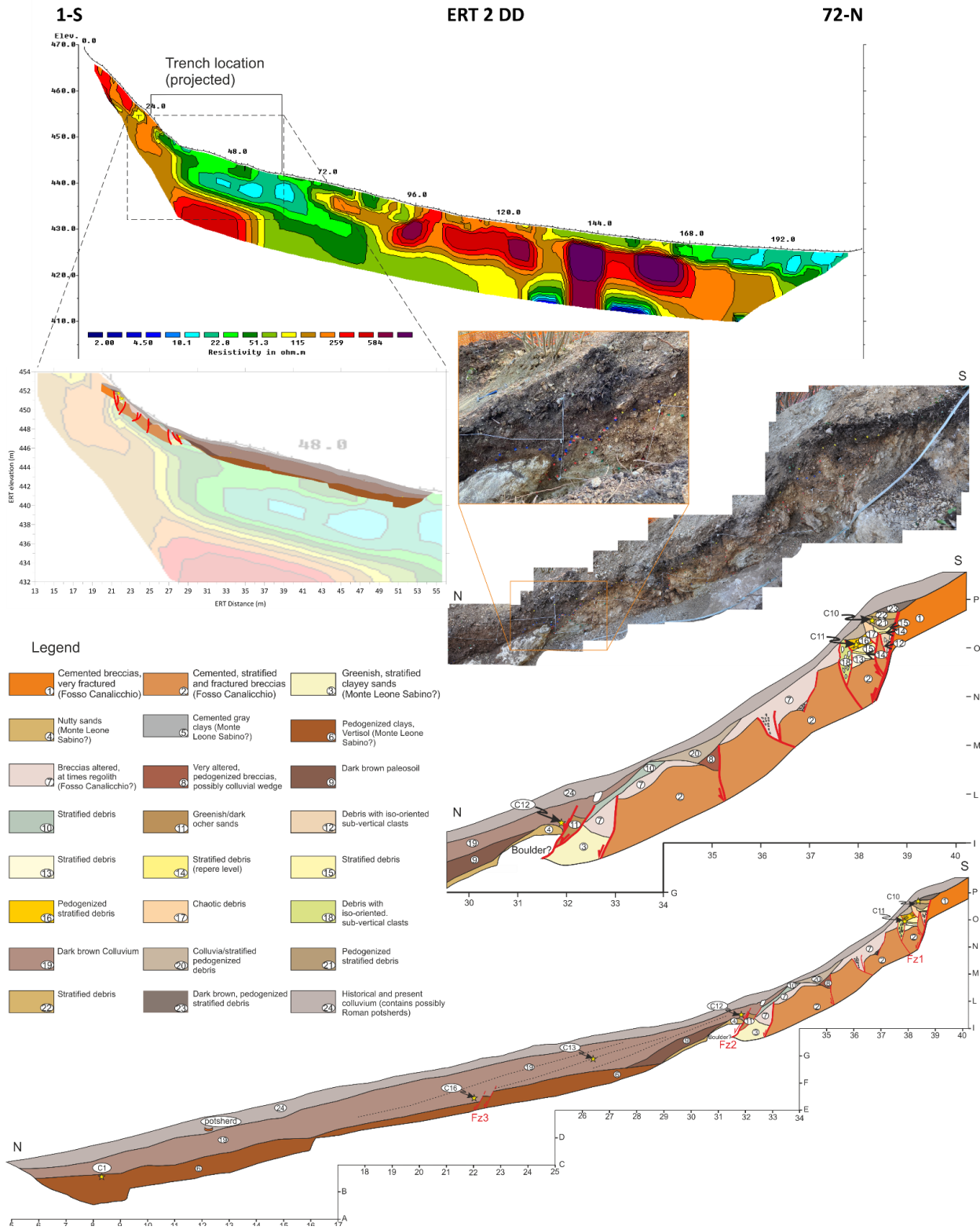
416 The second Sector under investigation is the Villa Stoli area, where ERT 02 and GPR 28 have been carried out (Fig. 8c; see
 417 Supplementary Data for GPR 28). In this case, only the tomography detected discontinuities due to tectonics. They are, in the
 418 southern part of the profile, corresponding to a wooded area where the GPR was not applied (Fig. 11). The anomalies detected,
 419 indeed, in the central-northern part of the ERT profile (Fig. 11) and in the GPR profile, correspond to the travertine slab found
 420 in the Villa Stoli Nord trench (see geology in Fig. 8c).

421 We excavated the Villa Stoli South trench for a length of 40 m, a depth of about 2 m and a width of 1 m. In the uphill, S part
 422 of the trench, we uncovered three major discontinuities, which were also detected by the ERT 02 survey. Figure 11 shows the
 423 stratigraphic log with tectonic elements.

424 The first discontinuity of the fault zone FZ1 offsets the Lower Pleistocene cemented breccia (Fosso Canalicchio Synthem, FC)
 425 and, with decimetric throw, also all the overlying deposits, until it is sutured by the current organic soil. Eight meters
 426 downstream, the elements of the FZ2 places the FC Synthem breccia (Unit 2) in contact with metric blocks of conglomerates
 427 associated with sandy-clayey sediments, interpreted as belonging to the Monteleone Sabino Synthem (MS). FZ2 fault zone
 428 upward cuts the overlying colluvium made of decarbonated dark reddish-brown soil (2.5YR 3/4) (Unit 19 in Fig. 11), whose
 429 AMS calibrated age (sample C12) is 21261-20961 BCE (95.4%). The faulted Unit indicates the occurrence of an event post
 430 21261-20961 BCE. This event is possibly correlated with the one observed in Sector 1, TR1, where a colluvial wedge dated
 431 back to 20919–20458 BCE. The two events TR1-1 and VS-1 in Figure 15 might therefore indicate the same paleoearthquake.

432 Starting from this point, the soil colluvium (Unit 19) thickens downwards, resting on a decarbonated clayey horizon (Unit 6 in
433 Fig. 11), developed on the clay-rich facies of the MS Synthem.

434 We identified another fault zone (FZ3) ten meters further downhill, toward the north. This fault offsets the interface between
435 the soil colluvium (Unit 19) and the pedogenized clay-rich horizon (Unit 6) with a throw up to 30 cm. The 14C calibrated age
436 of the younger deposits dislocated is 11835-11630 BCE (85.0%; Sample C16). This presumably means that a second seismic
437 event occurred after this date.



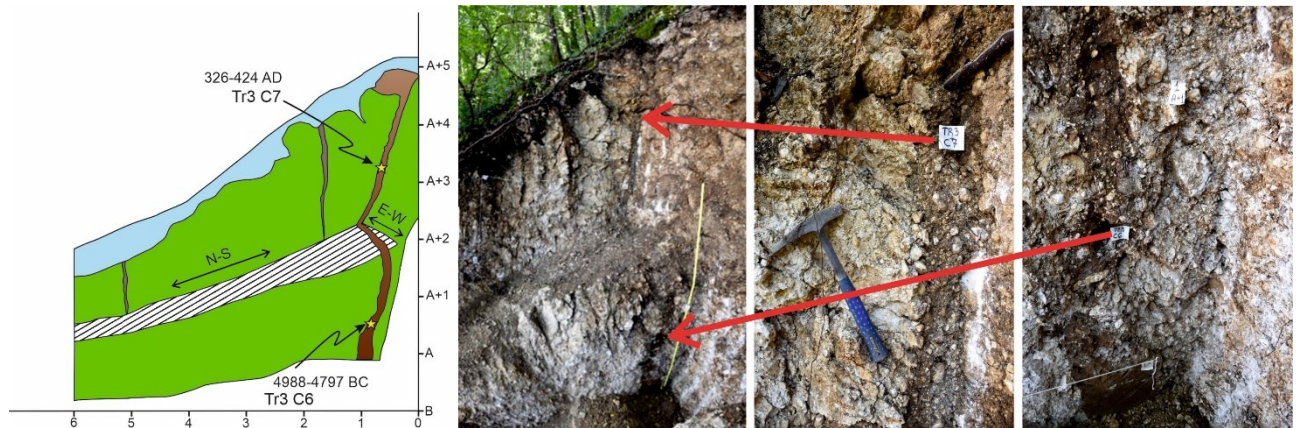
439
440
441
442
443
444
445
446
447
448
449
450
451
452

Figure 11: Southern Border Fault, investigations at Sector 2 – Villa Stoli; Above: ERT 02 profile; Middle: Photographic mosaic and stratigraphic log of the southern and upper part (first 10 m) of the E wall of the Villa Stoli Sud trench, including fault zones Fz1 and Fz2, and stratigraphic log superimposed on the southern part of the ERT 02 profile; Below: Stratigraphic log of the whole Villa Stoli South eastern trench wall.

4.3.3 Sector 3: Trenches TR3 and TR4

We selected the location of the trench TR3 based on geological and geomorphological evidence, without carrying out geophysical investigations. It was dug at the main slope break on the northern slope of the Castellaccio relief (Fig. 8d).

The excavation began where a fault outcrops in the cemented breccia of the Fosso Canalicchio Synthem (basal Lower Pleistocene in age), where the trench walls revealed open fractures filled by colluvial deposits. The breccias present sub-angular to angular clasts with generally centimetric up to decimetric diameters. The fracture, visible at progressive 1 m of the E trench wall (Fig. 12), is filled by brown paleosols that were sampled at different depths. The calibrated ages of the lower sample C06 and of the upper sample C07 resulted in 4988-4797 BCE (95.4%) and in 326-424 CE (78.6%) respectively. Since the filling of a seismic-induced open fracture supposedly occurs just after the event, an event should be dated just before 326-424 CE (event TR3-3 in Fig. 15) and another just before 4988-4797 BCE (event TR3-1 in Fig. 15).



453
454
455
456
457
458
459
460
461
462

Figure 12: Southern Border Fault, Sector 3; Left: tectonic fracture outcropping at the S end of the trench TR3, filled by colluvial deposits sampled in TR3 C7 (C07) and TR3 C6 (C06); calibrated C14 ages are, respectively, 326-424 CE (78.6%) and 4988-4797 BCE (95.4%); Right, log of the first 6 m of the E trench wall; “ledge” is a bench due to the backhoe excavation

From progressive 11 m toward N, there is an over one-meter-wide fault zone which brings in contact the Fosso Canalicchio Synthem with the overlying Monteleone Sabino Synthem (Fig. 13), the fault zone can be distinguished into two fault subzones.

The fault zones involve recent paleosols and colluvial deposits. Among them, Units 6 and 7 (Fig. 13), located only at the hanging wall of the FZ1, are evidently backtilted toward the fault. Unit 7 is a brown paleosol (7.5YR 5/4) developed on the sands of the Monteleone Sabino Synthem, with a calibrated age 4171-4036 BCE (60.9%; Sample C01). Above Unit 7 there is a soil colluvium (Unit 6) that contains small calcareous clasts, with a calibrated age 7729-7589 BCE (95.4%; Sample C02).

463 Going stratigraphically up section, Unit 5 is a dark brown colluvium (10YR 3/3) with a calibrated age 3711-3627 BCE (87.7%;
464 Sample C03), and Unit 4 is made of sub-angular-angular deposits, multi-centimetric in size, with a pedogenized matrix, with
465 a calibrated age 3243-3102 BCE (57.2%; Sample C04). The most downstream part of Unit 4 is thickened at the hanging wall
466 of the FZ1 (yellow star in the picture detail of Fig. 13) and because of this, it is interpreted as a colluvial wedge that formed
467 following the surface faulting event that tilted Unit 6 and 7. In this hypothesis, the underlying dark brown colluvium (Unit 5),
468 interrupted by FZ1, must have been deposited before the seismic event. The coseismic fault slip is 13 cm. All the above
469 considerations suggest the occurrence of a seismic event between 3627 and 3102 BCE. The age constraints for this event are
470 very similar to those available for the last event detected at APO-3 trench near Apoleggia along the N Border Fault, on the
471 opposite side of the Rieti Basin.

472 Moving N, the Monteleone Sabino Synthem outcrops with subvertical layers, parallel to the fault, probably because they were
473 dragged along the fault itself. These deposits are characterized by alternations of sandy and silty layers, rarely interspersed
474 with layers of fine gravel (millimetric clasts). Also, a system of mesoscale tectonic lineaments was recognized along the wall
475 of the trench, which are generally subparallel to the bedding. Therefore, we assume bed-parallel tectonic slip occurred here.

476 Towards progressive 24-26 m, the inclination of the Monteleone Sabino Synthem deposits decreases and the contact with a
477 pedogenized colluvium with clasts altered by pedogenesis (ghosts of clasts or “biscuit” clasts) has a slope of approximately
478 30° towards the valley (see Fig. 13).

479 Above the pedogenized colluvium, there is sharp contact with colluvial deposits characterized by frequent sub-rounded
480 calcareous clasts, with decimetric diameter, immersed in an abundant soil matrix. This contact, which is dipping about twenty
481 degrees towards the valley, becomes abruptly sub-horizontal in the N terminal zone of the trench.



NE SW NE SW

TR3 - East



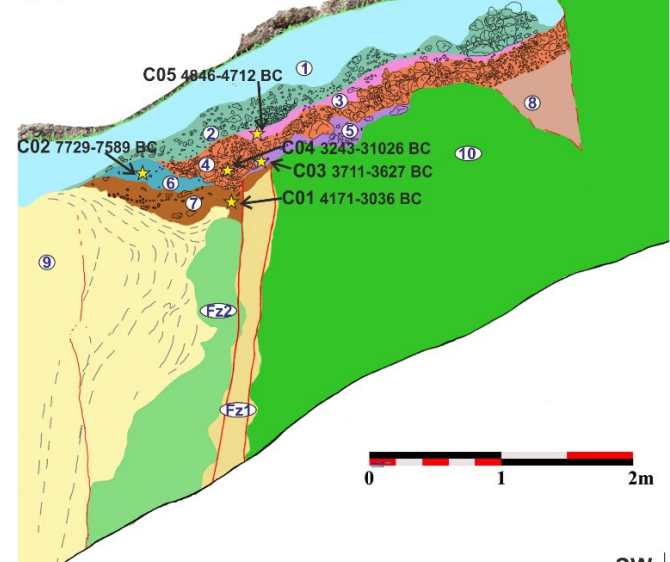
NE

Legend

1) Historical and present colluvium	6) Dark brown colluvium with scarce small calcareous clasts
2) Pedogenized debris deposit	7) Brown paleosol, developed on the Monteleone Sabino sands.
3) Dark brown colluvium	8) Breccias altered, at times regolith (Fosso Canalicchio?)
4) Debris deposit with sub-angular-angular clasts, multi-centimeter in size	
5) Dark brown colluvium	

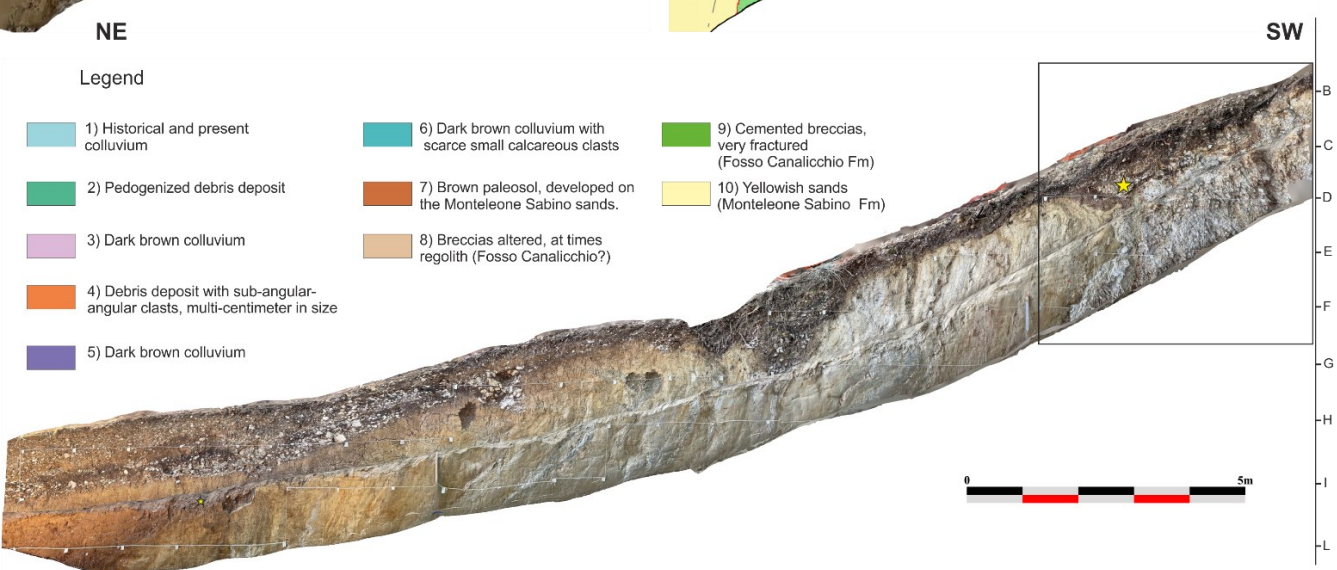
TR3 - East

Log detail from progressive 8 m to progressive 13 m



0 1 2m

SW

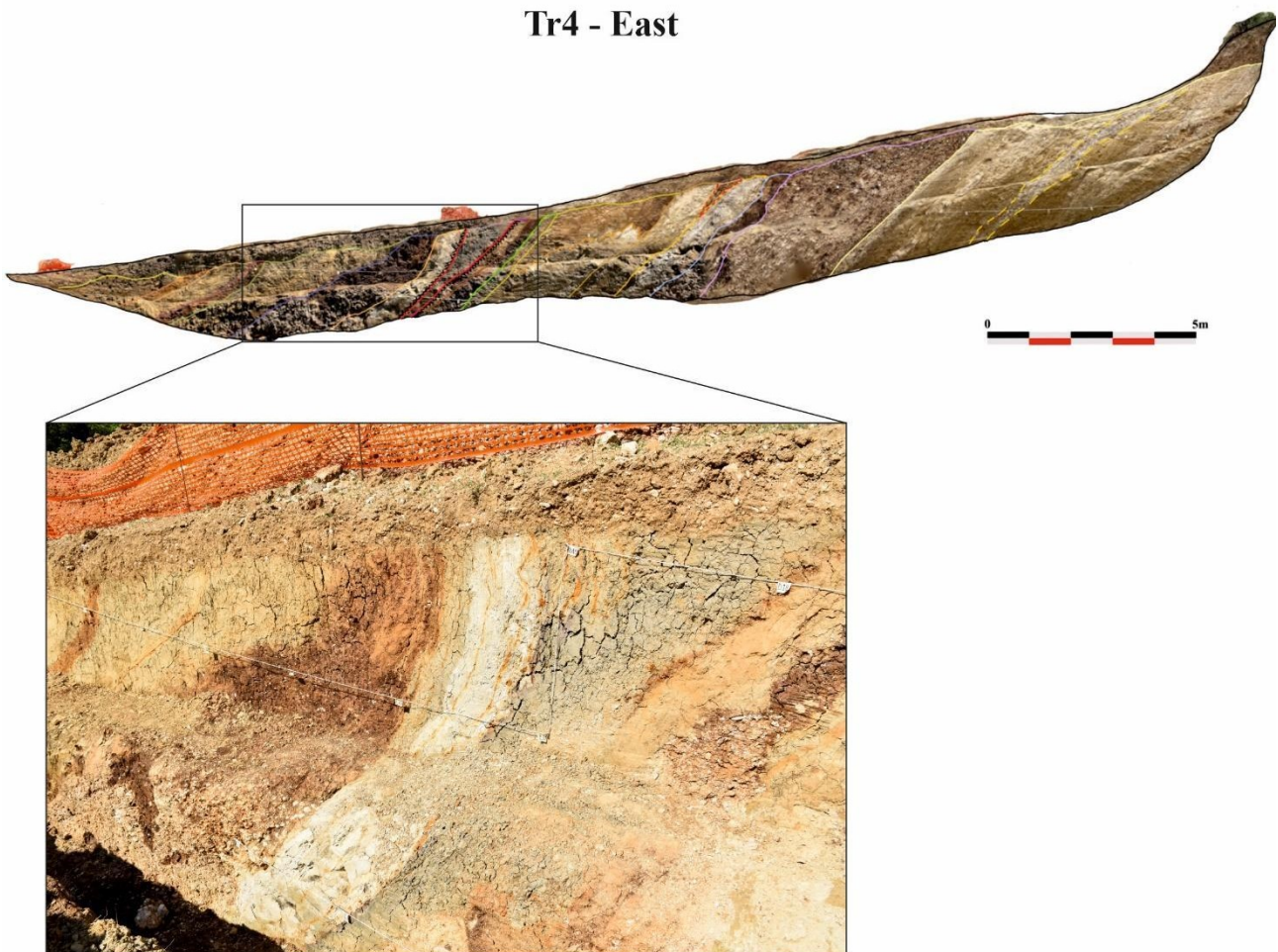


0 1 5m

11

483 **Figure 13: Southern Border Fault, Sector 3; portion (from progressive 8 m northwards to 26 m) of the E wall of the TR3 trench:**
484 **detail and log of the fault zone putting in contact the Fosso Canalicchio Synthem (Unit 10) with the Monteleone Sabino Synthem**
485 **(Unit 9); the stratigraphic log shows the deposits, the sampling points for AMS dating and the fault zones Fz1 and Fz2.**

486 In trench TR4, located north-east with respect to trench TR3 (see Fig. 8d) and 26 m long, we found the deposits of the
487 Monteleone Sabino Synthem dipping toward north-west, with slopes between 40° and 70° . Between the progressive 18 m and
488 19 m, gray silts diminish from the top to the bottom of the trench wall and are delimited by two fault surfaces (Fig. 14). In this
489 case, as in TR3, bedding-parallel slip is assumed. We observe that the faults are directly sealed by ploughed soil, and no
490 deposits younger than lower Pleistocene are involved in the deformation.



491
492 **Figure 14: Southern Border Fault, Sector 3; trench TR4, the bedding of the Monteleone Sabino Synthem dips between 40° and 70°**
493 **toward NW along the 26 m long trench; between the progressive 18 m and 19 m, gray silts diminishing from the top to the bottom**
494 **of the trench wall are delimited by two faults.**

495 **5 Discussion**

496 Here, we provide a critical discussion of the results obtained in the Rieti Basin, contextualized in the wider framework of the
497 Central Apennines. In fact, surface faulting events similar to those observed in the Rieti basin have been documented on nearby
498 Quaternary faults located near the SW flank of the Central Apennines (e.g., Leonessa Fault: Mildon et al.,
499 2022; Fiamignano Fault: Beck et al., 2018; Fucino Fault: Gori et al., 2017; Liri Fault: Maceroni et al., 2022). In particular,
500 slip histories recovered from the 36Cl data using Bayesian Monte Carlo Markov Chain (MCMC) modelling show that the
501 Leonessa Fault, Fiamignano Fault, Fucino Fault and Liri Fault exhibit a period of slip rate acceleration during the 7 to 5 kyr BP
502 and 2.5 to 1.5 Kyr BP time windows (Roberts et al., 2025). These are the same time intervals during which the Rieti Basin
503 faults generated the “Earthquake Sequences 1 and 2” based on the paleoseismic analyses described below.

504 The interpretation and correlation of paleoseismic data obtained during the study campaign on the Rieti Basin capable faults
505 conducted in 2021 - 2022 is necessarily limited due to the peculiar logistic and the stratigraphic/geomorphic field setting.
506 Nevertheless, we claim that a few elements of discussion can be pointed out.

507 First, we investigated selected areas identified based on administrative criteria. We conducted geophysical prospecting and
508 trenching on “active and capable faults” as defined by the Microzoning Guidelines of the Italian Government (Commissione
509 Tecnica per la Microzonazione Sismica, 2015). We worked in the framework of the “Scientific Collaboration Agreement
510 between the Extraordinary Commissioner for Reconstruction and the National Institute of Geophysics and Volcanology
511 (INGV)” for the redefinition of the Attention Zones of Active and Capable Faults emerging from the seismic microzonation
512 studies carried out in the Municipalities affected by the seismic events that occurred starting from 24 August 2016
513 (<https://sisma2016data.it/faglie-attive-e-capaci/>). For this reason, we aimed our investigations to specific technical targets, and
514 associated progressive deadlines, for the timely definition of the avoidance belts where the construction of new buildings and
515 the reconstruction of buildings damaged by the 2016-2017 seismic sequence had to be prevented.

516 Second, in the Rieti alluvial and lacustrine plain, literature data clearly show that the Late Holocene sedimentation rates are
517 tenfold the expected fault- slip rates (Guerrieri et al., 2006; Archer et al., 2019; Brunamonte et al. 2022). We confirmed this
518 conclusion also through our exploratory trenches in the N Study Area of the Rieti Basin. In the Rivodutri Area, we located two
519 trenches (Villaggio Santa Maria and Piedicolle trenches) in the lower part of the slopes, where ERT profiles suggested the
520 presence of faulting at shallow depth. In both trenches, we obtained AMS ages younger than 2000 years BP from colluvial and
521 alluvial deposits at 3 m below the ground surface. The presence of Roman pottery at the base of the trench walls confirmed
522 AMS dating. Therefore, our trenches did not reach the possible faults beneath the ground surface because of the excessive
523 thickness of very young historical deposits. In general, in the Rieti plain it is challenging to find suitable sites for paleoseismic
524 trenching; and it is not possible to expose faulted Holocene sediments in the high-resolution lacustrine stratigraphy. We
525 excavated all our 13 trenches at or near the bedrock-slope deposits contact, typically delimiting the reconstruction of
526 paleoseismic events with less well constrained chronologies and estimates of coseismic displacement.

527 Having this in mind, our new dataset, also compared with past paleoseismic analyses from Michetti et al. (1995), offers relevant
528 information on the paleoearthquake dates and magnitude, as discussed in the following sections.

529 **5.1 Post-Last Glacial Maximum (post-LGM) fault slip-rates and limestone bedrock scarp evolution in the Rieti Basin**
530 **landscape**

531 Data from our trench investigations confirmed the general model of post-LGM and Late Glacial to Holocene evolution for
532 bedrock fault scarps in the Meso-Cenozoic pelagic marly limestones of the Umbria-Marche-Sabina Sequence. As extensively
533 discussed in the literature (Bosi, 1975; Serva et al., 1986; Blumetti et al., 1993; Lorenzoni et al., 1993; Michetti et al., 1995;
534 Roberts et al., 2025), the morphological evidence of Holocene tectonic and seismic activity is very clear along the mountain
535 fronts carved in the Meso-Cenozoic Abruzzi carbonate platforms.

536 During the Last Glacial Maximum, the high elevations of the Central Apennines (up to 2900 m) supported valley glaciers, as
537 indicated by moraines and associated glacial landforms. Beyond the glaciated zones, periglacial conditions dominated. On
538 slopes composed of pure carbonate bedrock, rapid erosion and sedimentation—exceeding 0.2–0.4 mm yr⁻¹ (Tucker et al.,
539 2011)—favored the development of alluvial fans emerging from ice-free valleys. These rates surpassed typical fault throw
540 rates (Roberts and Michetti, 2004), as proved by fan surfaces and colluvial slopes graded to adjacent footwall bedrock.
541 Following glacier retreat, the establishment of temperate vegetation stabilized both fans and slopes, while stream discharge
542 declined, producing the smooth hillsides characteristic of former periglacial landscapes. Fan surfaces, bedrock slopes, and
543 moraines are mantled by thin soils (0.5–1.0 m) enriched in organic matter and locally containing volcanic components
544 deposited during and after deglaciation. Terminal moraines are frequently overlain by fluvial outwash or lacustrine deposits,
545 which often include paleo-vegetation and volcanic ash suitable for radiocarbon dating and tephrochronology. These
546 chronological datasets enable robust age determinations and correlations with climate records from Tyrrhenian Sea cores and
547 other archives. The final major phase of glacial retreat occurred ca. 18–16 ka, coinciding with a marked $\delta^{18}\text{O}$ shift in marine
548 records, signaling a major climatic transition. Presently, normal fault scarps dissect these glaciation-related landscapes,
549 exposing minimally degraded Mesozoic carbonate platform bedrock in footwalls. Conversely, marly-limestone bedrock of the
550 Umbria-Marche-Sabina pelagic domain exhibits higher modern erosion rates than the Abruzzi carbonate platform ($0.016 \pm$
551 0.005 mm yr⁻¹; Tucker et al., 2011). Prominent fault scarps in basins such as Rieti, Leonessa, and Norcia occur only where
552 pure carbonate formations (e.g., Calcare Massiccio and Maiolica Fms.) are exposed.

553 The same is not true for the Rieti Basin and other Quaternary basins in the Umbria-Marche-Sabina sector (such as the Norcia,
554 Leonessa and Colfiorito basins; Messina et al., 2002; Mildon et al., 2022), where the presence of forest cover on the slopes
555 indicates the development of pedogenetic and colluvial processes on the material supplied by the Mesozoic marly-clay-rich
556 units.

557 Moreover, human impact on the mountain slopes through deforestation and agriculture generated a significant increase in the
558 sedimentation rates of slope deposits since the early stage of the Roman Empire, and thereafter (Lorenzoni et al., 1993; Michetti
559 et al., 1995; Borrelli et al., 2014). Stratigraphic and geoarchaeological data at La Casetta site clearly document this

560 anthropogenic impact, with meters of Roman to Middle Ages slope deposits containing abundant and well dated pottery
561 remains.

562 This is therefore the reason why bedrock fault scarps in the Rieti Basin are discontinuous and relatively subdued. As already
563 mentioned, the selection of trench sites in our study was affected by logistic constraints, since the primary goal of our study
564 was the characterization of capable faults in urban areas, aiming at post-emergency reconstruction. However, we successfully
565 investigated two of these bedrock fault scarps, one along the N border fault at Apoleggia sector, and the second along the E
566 master fault at Cantalice sector. Trenching and geophysical prospecting in the Cantalice area, Sector 2, shows faulted historical
567 colluvial deposits against the Scaglia Fm. fault plane. The measured slip-rate of 0.25 mm/yr is a minimum, because our
568 trenching did not reach the base of historical slope sediments. We draw a similar conclusion also at Apoleggia. Here we
569 observed a synthetic fault splay in the hanging wall of the bedrock fault scarp. Therefore, the measured slip-rate of 0.29 mm/yr
570 is also a minimum estimate.

571 Nevertheless, these values are meaningful because we have both morphological and stratigraphic constraints. These new post-
572 glacial fault slip-rate data confirm the previous estimates available in the Rieti Basin. Roberts and Michetti (2004) measured
573 0.27 mm/yr at a site N of Rivodutri along the Rieti Eastern Border Fault; and Michetti et al. (1995) documented 0.4 mm/yr
574 over the Holocene at the Piedicolle trench site along the Northern Border Fault.

575 Several Late Quaternary faults in Central Italy share similar post-glacial slip-rates (Roberts et al., 2025; Lombardi et al., 2025).
576 For instance, the Mt. Morrone Fault (0.20 – 0.40 mm/yr; Puliti et al., 2024); the Paganica Fault that generated the April 6,
577 2009, Mw 6.0 earthquake (0.25 – 0.30 mm/yr; Cinti et al., 2011) the Montereale Fault which ruptured during the January 16,
578 1703, Mw 6.0, earthquake (0.30 – 0.40 mm/yr; Cinti et al., 2018) and the Mt. Vettore–Mt. Bove normal fault system source of
579 the Mw 6.5 Norcia earthquake of October 30, 2016 (minimum 0.26 – 0.38 mm/yr; Cinti et al., 2019). More recent slip rates
580 estimates for the Mt. Vettore Fault are 0.8-1 mm/yr (Puliti et al 2020); 0.7-1.2 mm/yr (based on ^{36}Cl exposure dating of
581 bedrock fault plane; Pousse Beltran et al. 2022); ranging from a minimum of 0.4 to a maximum of 1.3 mm/yr (Galli et al.,
582 2019).

583 **5.2 The paleoseismic history of the Rieti Basin: a possible pattern in the earthquake sequence?**

584 We compiled the paleo-earthquakes identified in the trenches with those recognized by Michetti et al. (1995) (i.e., the
585 Piedicolle and La Casetta trenches, PDC and CAS, respectively, with original Geochron Lab. radiocarbon dates recalibrated
586 using the IntCal20 curve) and summarized all the data in the space-time diagram in Figure 15.

587 Red bars are the time spans of the calibrated ages, defining the terminus *ante-* and/or *post-quem* for earthquakes (see Table 2).
588 Some paleo-events are tightly constrained in time (e.g., CUC-2), whereas in other cases we have less robust chronological
589 constraints, and in some cases can only bracket the timing of the paleoseismic events.

590 We highlighted five events, here coded as A to E, which are chronologically well-constrained (i.e., black boxes in Figure 15),
591 plus one less-constrained additional event (F in Figure 15). The six events do not overlap in time, thus possibly representing
592 distinct earthquakes. Correlation of paleoseismic events recognized in different trench sites are inherently speculative in nature.

593 Moreover, for the Rieti Basin we consider these correlations unlikely, given the large chronological uncertainty. Nevertheless,
594 we think that these correlations should be taken seriously into account, as they depict a conservative scenario in terms of
595 reconstructing the maximum credible earthquake magnitude and associated seismic hazard. Below we summarize the evidence
596 driving our interpretation, supplemented with constraints from historical catalogues, and we discuss potential ruptures of the
597 whole Rieti Basin Fault segment.

598 Event A is constrained at trench TR3 in the SE margin of the basin; the coseismic movements that occurred over time along
599 the identified fault (Fig. 12) cyclically determined the reopening of the fracture, which was repeatedly filled with *colluvia*. The
600 younger age obtained from the *colluvia* trapped in the fracture is 326-424 CE (1624-1526 cal BP). No event in the historical
601 seismic catalogue matches with our Event A.

602 A few centuries before, a strong event is reported to have occurred in the Rieti area in 76 BCE (Guidoboni et al., 2018, 2019).
603 Obsequens Iulius (1910) stated:

604 “*Reate terrae motu aedes sacrae in oppido agrisque commotae. Saxa quibus forum stratum erat, discussa.*
605 *Pontes interrupti. Ripae [prae] labentis fluminis in aquam provolutae, fremitus inferni exauditi et post*
606 *paucos dies, quae concussa erant, corruerunt*”

607 (Due to the earthquake, the sacred buildings in the town and the fields were moved. The stones with which
608 the market was laid were broken up. Bridges broken. The banks of the flowing river were thrown into the
609 water, the roar of hell was heard, and after a few days those that had been shaken collapsed).

610

611 **Table 2: Attributes summary of the paleo-earthquakes identified in the trenches excavated in the Rieti Basin; the “notes” column**
612 **refers to the possible ruptures of the whole Rieti Fault segment as described in the text; asterisks mark the events that “control”**
613 **Event A, B, C, D, E; F; the others are the possible correlations.**

Trench	Earthquake	Younger than	Older than	Offset	Notes
TR3	3	-	326-424 CE (1624-1526 cal BP)	-	A*
TR3	2	3711-3627 BCE (5661-5577 cal BP)	3243-3102 BCE (5193-5052 cal BP)	13 cm (min)	C
TR3	1	-	4988-4797 BCE (6938-6747 cal BP)	-	D*
TR1	2	3811–3701 BCE (5761-5651 cal BP)	-	30 cm	A, B, C

TR1	1	-	20919-20458 BCE (22869-22408 cal BP)	15 cm (min)	F*
VS	2	11835-11630 BCE (13785-13580 cal BP)	-	38 cm	B, C, D, E
VS	1	21261-20961 BCE (23211-22911 cal BP)	-	78 cm	B, C, D, E, F
CUC	2	591-408 BCE (2541-2358 cal BP)	401-351 BCE (2351-2301 cal BP)	53 cm	B*
CUC	1	-	591-408 BCE (2541-2358 cal BP)	34 cm	C, D, E, F
CAS	1	5623-5205 BCE (7573-7155 cal BP)	3999-3640 BCE (5949-5590 cal BP)	80-100 cm	D
PDC	2	-	1971-1517 BCE (3921-3467 cal BP)	100 cm	C, D, E, F
PDC	1	4446-3794 BCE (6396-5744 cal BP)	-	90 cm	A, B, C
APO T2	2	3533-3370 BCE (5483-5320 cal BP)	3110-2907 BCE (5060-4857 cal BP)	22 cm (min)	C*
APO T2	1	11127-10795 BCE (13077-12745 cal BP)	5664-5512 BCE (7614-7462 cal BP)	15 cm	E*
CAM	1	17415-16872 BCE (19365-18822 cal BP)	-	27 cm (last event)	A, B, C, D, E

614

615 In the Italian seismic catalogue, the 76 BCE event has an Epicentral Intensity X and an intensity-derived magnitude Mw 6.4.
616 Guidoboni et al., 2018). Guidoboni et al. (2018, 2019), based on the only historical source available, place the epicenter in
617 the town of Rieti, but its exact location could be anywhere in the basin area, or in the SE part of the basin, like the M 5.5 event
618 occurred in 1898 CE (Rovida et al., 2022; Comerci et al., 2003). Chronological constraints obtained from the trenches indicate
619 that the earthquakes identified in TR1 (S margin) or PDC and CAM (N margin) overlap with the 76 BCE, even though the
620 dating uncertainties are high.

621 Regarding the extension of faulting associated with Event A, and possible involvement of multiple fault splays in the Rieti
622 Basin, we note that paleo-earthquakes consistent with the chronology of Event A are found in trenches TR1 (S margin of the
623 basin), PDC and CAM (N margin). We are indeed quite confident that Event A did not produce faulting at APO T2 Site, since
624 the top of Unit 5 seals the deformation there and younger deposits are not faulted (Fig. 3).

625 Event B is tightly constrained at trench CUC (E margin of the basin); the earthquake occurred between 591-408 BCE (2541-
626 2358 cal BP) and 401-351 BCE (2351-2301 cal BP), with an offset of 53 cm. A tentative hypothesis about a rupture affecting
627 the E master fault and multiple fault splays in its hanging wall is supported by paleo-earthquakes identified at trenches TR1,
628 VS, PDC and CAM; however, like Event A, such correlations seem highly speculative.

629 In the time span between 3 and 5 kyr BCE, all of the three investigated margins of the basin moved: the N margin hosted Event
630 C, constrained at APO T2, dating between 3533-3370 BCE (5483-5320 cal BP) and 3110-2907 BCE (5060-4857 cal BP) and
631 with a minimum offset of 22 cm. Trenching at La Casetta site shows evidence for the movement of the E master fault, dated
632 between 5623-5205 BCE (7573-7155 cal BP) and 3999-3640 BCE (5949-5590 cal BP). The movement of the S margin is
633 constrained at TR3 Site, where two earthquakes have been recognized: the one dated between 3711-3627 BCE (5661-5577 cal
634 BP) and 3243-3102 BCE (5193-5052 cal BP) has a good overlap with Event C, while the earthquake dated at 4988-4797 BCE
635 (6938-6747 cal BP) is tightly constrained and identified as Event D. We can confidently claim that Events C and D are two
636 distinct earthquakes, since the date ranges do not overlap. Therefore, Events C and D likely did rupture the whole length of
637 the ca. 21 km long Rieti Basin with a Mw in the order of 6.5. This is consistent with coseismic displacement of more than 50
638 cm observed at CUC (Event D, CUC1; Fig. 15), and in the order of 1 m observed at PDC (Events C and D, PDC1 and PDC2;
639 Fig. 15).

640 Event E activated the N margin and is broadly constrained at APO T2 Site (date range between 11127-10795 and 5664-5512
641 BCE, i.e., 13077-12745 and 7614-7462 cal BP). Like for the other events, in this case weak correlations with movements on
642 the other margins of the basin are possible.

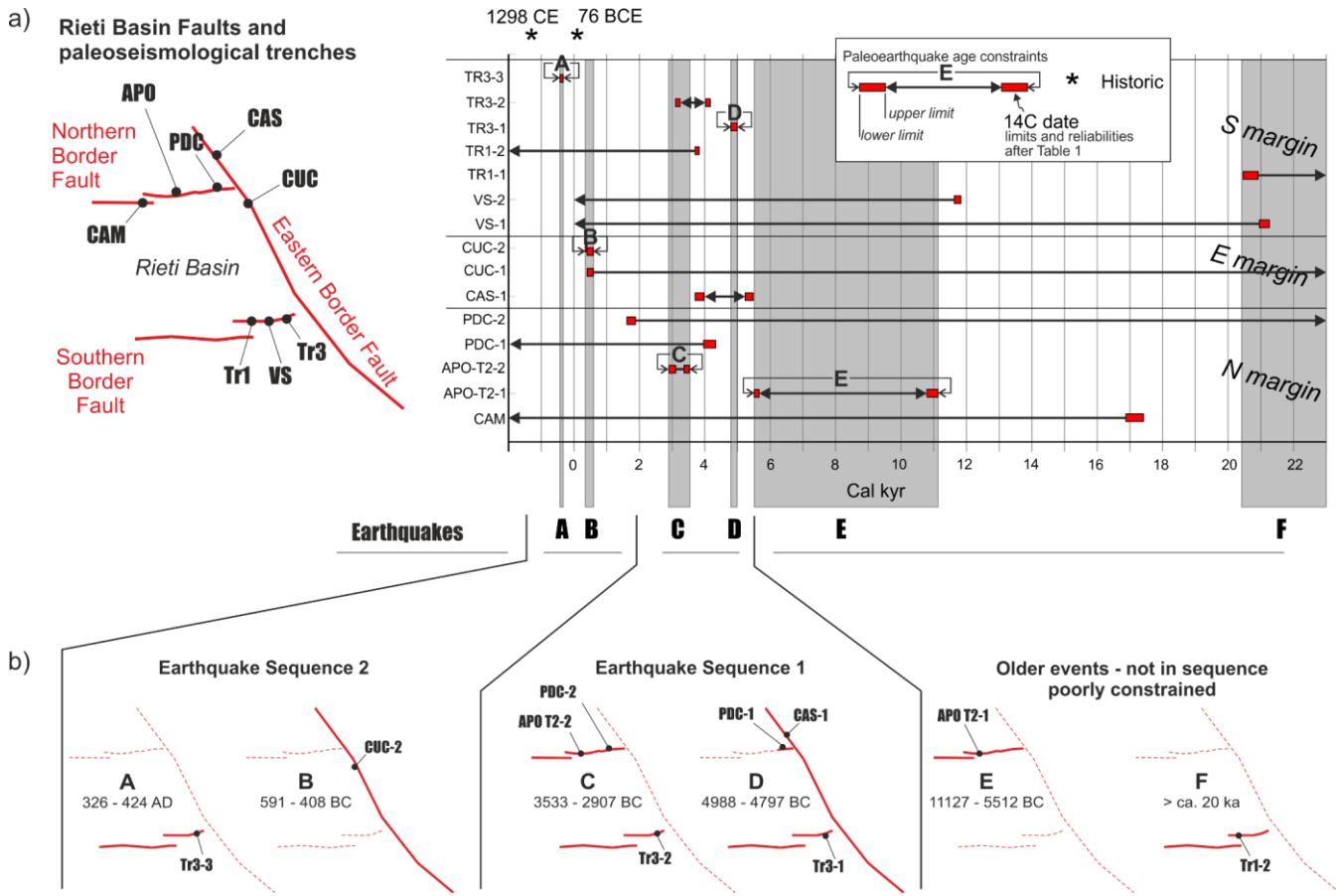


Figure 15: a) Space-time diagram at the basin scale; on the ordinates the acronym of the earthquakes recognized in each trench (from Table 2); each horizontal bar represents the temporal constraints to the occurrence of each earthquake; black boxes indicate well-constrained events, and the grey transparent bars are highlighting possible correlations across trenches; b) summary of the sequence of fault ruptures along the basin-bounding faults, based on well-constrained events (thick continuous lines indicate fault ruptures; thin dashed lines, not assessed).

Finally, Event F involved the S margin of the basin; it is constrained at TR1, with an estimated age older than 20919–20458 BCE (22869–22408 cal BP). This event is also responsible for the dislocation of the colluvial Unit 19 dated 21261–20961 BCE (23211–22911 cal BP) in the trench of Villa Stoli (Sample Ri12; event VS1).

Figure 15b summarizes the overall picture emerging from this complex pattern of fault ruptures, given the uncertainties of both the age dating and possible across-trenches correlations. Seven earthquakes have an age bracketed in time, three referring to the S margin (trench TR3), two on the E margin (events CUC-2 and CAS-1) and two on the N margin (trench APO T2). The average recurrence interval is of a few millennia on all the segments; given fault length and the long-term slip rate, the recurrence intervals obtained in our study are consistent with observations on a global scale (Mouslopoulou et al., 2025). If we only rely on the chronologically well-constrained events correlated across-trenches, these indicate two sequences of rupturing events that follow a similar spatial pattern (i.e., Earthquake Sequences 1 and 2 in Fig. 15b). With the term “earthquake

659 sequence" we refer to a series of characteristic earthquakes rupturing adjacent fault segments or adjacent faults over a short
660 time period.

661 Earthquake Sequence 1 started with the rupture of the main fault bordering the basin, the Eastern Border Fault, and of the
662 Southern Border Fault around 4988 – 4797 BCE (6938-6747 cal BP; Event D). Possibly, also the easternmost tip of the
663 Northern Border Fault ruptured, as recorded at the PDC trench (Michetti et al., 1995). The sequence ended up with the rupture
664 of the Northern and Southern Border Faults around 3533 – 2907 BCE (5483-4857 cal BP).

665 After an apparent period of quiescence, the inception of Earthquake Sequence 2 is dated 591 – 408 BCE (2541-2358 cal BP),
666 when the Eastern Border Fault ruptured with a major earthquake (Event C) that was later followed by the movement of the
667 Southern Border Fault at 326 – 424 CE (1624-1526 cal BP).

668 The general recurring scheme here is that for each sequence, a main rupture of the Eastern Border Fault is later followed by
669 movements on the other two structures.

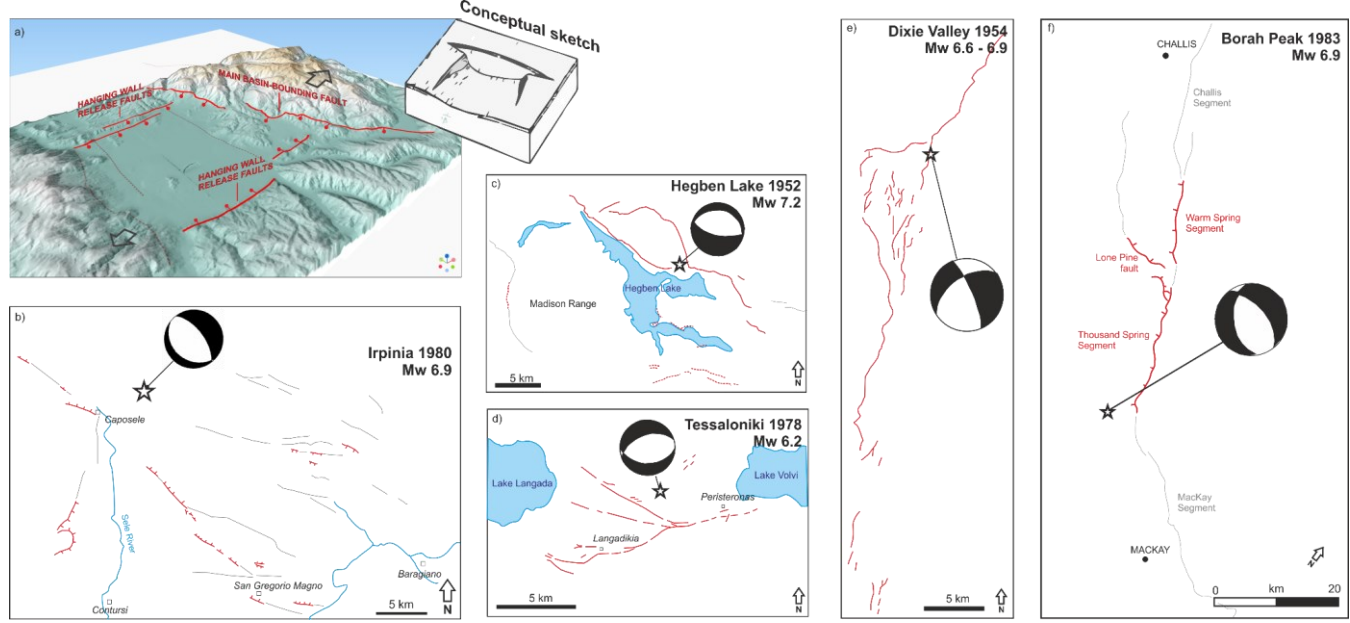
670 The structural setting of the Rieti Basin might shed some light on such behavior. In fact, the basin is bounded to the east by a
671 main west-dipping fault, whereas relatively short orthogonal faults bound it to the north and to the south. The latter faults are
672 constrained within the hanging wall block of the main Eastern Border Fault. Such a fault architecture can be interpreted in
673 terms of a hanging wall release faults model (*sensu* Destro, 1995; Figure 16a). The role of release faults is to accommodate
674 the hanging wall deformation resulting from a bow-shaped profile of cumulative slip along a fault strike. If a significant
675 displacement gradient exists along the fault strike, then resultant orthogonal extension can be accommodated by release faults.
676 This is the case of the extensional faults in the Central and Southern Apennines, where structural inheritance from previous
677 tectonic phases (Capotorti and Muraro, 2024) results in relatively short faults with high displacement gradients (e.g., Roberts
678 and Michetti, 2004; Papanikolaou and Roberts, 2007; Porreca et al., 2020). The faults bounding the Rieti Basin are indeed
679 located close to inherited rift-related faults. To the west, the basin bounding fault runs almost along the inherited Sabina
680 Paleofault (Galluzzo and Santantonio, 2002). To the east, the main basin-bounding fault is running at the margin of a series of
681 aligned Mesozoic structural highs (i.e., the so-called pelagic Carbonate Platforms - PCP; specifically, the Lisciano, Mt. Rosato
682 and Polino ones; Capotorti and Muraro, 2024).

683 In this line, the proposed rupture sequence would originate from the entire rupture of the Eastern Border Fault: the resulting
684 stress loading on the other two receiving faults would result in a later re-adjustment of the strain field by means of one or more
685 earthquakes on the hanging wall release faults (e.g., Mildon et al., 2017; Valentini et al., 2024).

686 The architecture of the faults bordering the Rieti basin is apparently odd, with systems of normal faults striking at ca. 60°-
687 120°. Nonetheless, other well-documented examples worldwide (Figure 16b-e) highlight that normal faulting events can result
688 in a surprisingly complex pattern of deformation and surface ruptures, with faults trending at high angles to each other. This
689 mainly results from i) oblique extension and/or ii) the presence of inherited structures partly misoriented with respect to the
690 orientation of the stress field but may still be compliant for future re-activations.

691 As a general consideration, the rupture of the whole eastern master fault of the Rieti Basin seems to be the only scenario
692 compatible with the Mw 6.4 estimated by the CFTI5Med catalogue (Guidoboni et al., 2018, 2019) for the 76 BCE event, or

693 with the Mw 6.26 estimated by the CPTI15 catalogue (Rovida et al., 2022) for the 1298 event. In summary, the paleoseismic
 694 history described above suggests a maximum magnitude in the order of Mw 6.5. We discuss below that this interpretation
 695 agrees with the available data from surface faulting events that occurred in Central and Southern Italy during the instrumental
 696 era, and in particular over the past 45 years.



697
 698 **Figure 16:** a) a 3D perspective on the Rieti basin with the studied faults and a conceptual scheme (after Destro, 1995, modified)
 699 illustrating the structural interpretation for the area, with the E Fault as Master Fault of the Rieti Basin and the N and S Faults as
 700 hanging wall release faults; b) to f): the complexity of the surface fracture pattern occurred during well-documented ruptures
 701 accompanying Mw 6.2 – 7.2 normal faulting earthquakes in Italy, Greece and the US Basin and Range Province, with the calculated
 702 moment tensor solutions (Doser, 1984; 1986; Crone, 1987; Liotier, 1989; Giardini, 1993).

703 5.3 Fault displacement hazard in the Rieti basin

704 The paleo-earthquakes identified in the Rieti basin show offsets in the order of few cm to 1 m (Table 2). We consider these
 705 values consistent with the seismic potential of the region. In a broader perspective, the Rieti basin belongs to the seismotectonic
 706 setting of the Central-Southern Apennines, which in the last decades were repeatedly hit by groundbreaking earthquakes.
 707 As illustrated in Table 3, the Colfiorito 1997, L'Aquila 2009, Amatrice 2016 and Visso 2016 earthquakes had magnitude in
 708 the Mw 6.0 range and resulted in maximum displacement of 20 cm (Vittori et al., 2011; Boncio et al., 2012; Pucci et al., 2017).
 709 The much stronger Fucino 1915, Irpinia 1980 and Norcia 2016 earthquakes (Mw 6.5-6.9) instead generated metric
 710 displacements (max values 210 cm; Pantosti and Valensise, 1990; Michetti et al., 1996; Villani et al., 2018).
 711

Table 3: Ground rupture parameters for recent earthquake surface faulting along normal faults in the Central and Southern Apennines. SRL = Earthquake Surface Rupture Length

Earthquake (dd/mm/yyyy)	Mw	SRL (Km)	MAX Disp (m)	Source
Fucino 13/01/1915	7.0	27 (36)*	1.0*	Michetti et al., 1996; Galadini and Galli, 1999*
Irpinia 23/11/1980	6.9	30	1.3	Pantosti and Valensise, 1990
Colfiorito 26/09/1997	6.0	12	0.08	Guerrieri et al., 2010
Sellano 14/10/1997	5.6	1.7	0.04	Guerrieri et al., 2010
Lauria 09/09/1998	5.6	0.2	0.02	Michetti et al., 2000
L'Aquila 06/04/2009	6.1	13.0	0.15	Vittori et al., 2011
Amatrice 24/08/2016	6.0	5.2	0.20	Pucci et al., 2017
Visso 28/10/2016	6.0	7.0	0.4	Scognamiglio et al., 2018
Norcia 30/10/2016	6.5	21.9	2.4	Villani et al., 2018

716 The hypothetical rupture of the whole Rieti Fault would result in a surface faulting length of ca. 21 km. Using literature
 717 empirical relations (e.g., Wells and Coppersmith, 1994; Pavlides and Caputo, 2004), the corresponding magnitude would be
 718 around 6.5. This is consistent with the coseismic ruptures in Table 3, in particular with those observed during the October 30,
 719 2016, Mw 6.5, Norcia earthquake.

720 As a further speculation, we observe that in case of Mw 6.5 events, surface ruptures along the W margin of the Basin would
 721 not be seen as a surprise. In fact, the 2016 Mw 6.5 Norcia earthquake generated surface faulting several km west of the Mt.
 722 Vettore master fault, including antithetic ruptures that affected the San Benedetto subsurface road tunnel located ca. 8 km west
 723 of the master fault (Galli et al., 2020).

724 On the other hand, Table 3 shows that the threshold for surface faulting during shallow crustal normal faulting earthquakes in
 725 the Central - Southern Apennines is ca. Mw 5.6. Again, this is consistent with observations from recent moderate magnitude
 726 events in the Rieti Basin. The June 27th, 1898, Santa Rufina event (Mw 5.5; Io VIII-IX MCS; Comerci et al., 2003) generated
 727 ground fractures E of Rieti. According to Moderni (1899), near Santa Rufina “seven large and long cracks” had formed in
 728 1898, parallel and close to each other; while five similar long cracks had formed 2-3 km W of Cupello. However, during the
 729 December 31st, 1948, Rivodutri event (Mw 5.3; Io VIII MCS; Bernardini et al., 2013), near the NE border of the basin, we
 730 have no report of ground fractures.

731 **6 Conclusions**

732 In this paper, we present new insights regarding the paleoseismic history of the Rieti Basin in Central Italy, derived from the
733 excavation of 17 paleoseismic trenches. Our work represents the first comprehensive characterization of the seismic hazard of
734 the Rieti Basin, which so far has been underdocumented compared to other areas of the Italian Apennines.

735 Through extensive fieldwork and analyses, we identified and chronologically constrained up to 15 paleo-earthquakes that
736 generated surface faulting on three sides of the box-shaped Rieti basin during the last ca. 20 ka. These results provide a baseline
737 of tectonic activity in the region that was not known prior to this work.

738 Considering the spatio-temporal distribution of the faulting events, we propose a temporal development characterized by the
739 earthquake rupture of the Eastern Border Fault, followed by seismic events either on the northern or southern border faults.

740 This pattern is consistent with the structural architecture of the basin, which comprises two sets of nearly orthogonal faults.

741 Our results indicate that the maximum credible earthquake in the Rieti Basin is in the order of magnitude Mw 6.5, which is
742 consistent with the general setting of the Central Apennines. Given the resolution of chronological constraints obtainable with
743 radiocarbon dating techniques in paleoseismic trenches, we cannot disentangle the occurrence of a single earthquake as
744 compared to multiple earthquakes occurring over a short time interval (like the 2016 seismic sequence). Additionally,
745 paleoseismic data inherently focus on surface-rupturing earthquakes, thus aliasing smaller seismic events, which however
746 could have caused significant damage.

747 Our study reinforces the need for detailed paleoseismic studies in a careful evaluation of the seismic hazard in such a densely
748 populated region. The study of capable faults affecting urbanized zones indeed provides valuable contexts that should inform
749 decision-making; we argue that conducting similar projects like ours could benefit other areas in and beyond the Italian
750 territory.

751 **Author contribution**

752 Conceptualization and writing: FL, AMM, MFF, ES, VC, MCac, AMB. Field work, geological mapping, trenching and
753 logging: FL, AMM, MFF, ES, VC, MCac, AMB, PDM, FF, RG, PL, ASF, MP, KN, GT, FT, AP, FF, MG, FM, RNap, RNav,
754 RP, LMP, MR, AR, VR. Geophysical data acquisition and processing: LMP, VM, VR, VS, SU. Scientific discussion and text
755 revision: KN, AZ, GB, MCol, LG, PDM.

756 **Code/Data availability**

757 All the data are publicly available in this work and in the Supplementary Material. The data presented are included in the
758 microzonation studies carried out in the municipalities of Central Italy affected by the seismic events starting from August 24,
759 2016, as provided by Ordinance No. 24 of May 12, 2017, issued by the Extraordinary Commissioner.

761 With Ordinance No. 55, Article 5, "Amendments to Ordinance No. 24 of May 12, 2017," the general criteria were approved
762 for the use of Level 3 Seismic Microzonation studies in the reconstruction of the areas affected by the seismic events starting
763 from August 24, 2016. All the reports and data are publicly available at <https://sisma2016data.it/microzonazione/>)in Italian
764 (last accessed on the 29th, May 2025).

765 **Competing interests**

766 The Authors declare that they have no conflict of interest.

767 **Acknowledgements**

768 We are grateful to the owners of the land where we conducted geophysical prospecting and trench investigations. The
769 assistance of the Rivodutri, Cantalice, Rieti and Cittaducale Municipalities is gratefully acknowledged. Special thanks to
770 Matteo Carrozzoni, Geologist at "Commissario Straordinario Ricostruzione Sisma 2016", for the invaluable support to this
771 project: without him our research would have been simply impossible. Thanks to Francesco Chiaretti and Domenico "Mimmo"
772 Marchetti, authors of the local microzoning studies, for sharing their expertise and scientific discussion. We are grateful to
773 Enzo Sepe, INGV leader of the 2016 post-seismic capable fault project, indeed a scientific leader; and to Carlo Doglioni,
774 INGV President, who strongly believed in the realization of this project.

775 **Financial support**

776 The agreements of scientific collaboration between INGV, ISPRA, and Università degli studi dell'Insubria "Ridefinizione
777 delle Zone di Attenzione delle Faglie Attive e Capaci emerse dagli studi di microzonazione sismica effettuati nel territorio
778 comunale di Cittaducale (RI) e Rieti, interessati dagli eventi sismici verificatisi a far data dal 24 agosto 2016" signed on
779 December 2020 and "Aggiornamento degli studi di microzonazione sismica a seguito degli approfondimenti dedicati alle zone
780 delle faglie attive e capaci presenti nei territori dei Centri abitati di Rieti e Cittaducale (RI)" signed on April 2022 provided
781 funding and the legal framework for the paleoseismic investigations in the Rieti Basin carried out by ISPRA and Università
782 degli Studi dell'Insubria.

783 Research funded by European Union – NextGenerationEU – Mission 4 "Education and Research" – Component 2 "From
784 Research to Business" – Investment 3.1 "Fund for the realization of an integrated system of research and innovation
785 infrastructures" – Project IR0000037 – GeoSciences IR - CUP I53C22000800006

786 K. Nicoll acknowledges support and funding from the USA-Italy Fulbright Program.

787 **References**

788 Archer, C., Noble, P., Rosen, M., Sagnotti, L., Florindo, F., Mensing, S., Piovesan, G., and Michetti, A. M.: Lakes as
789 paleoseismic records in a seismically-active, low-relief area (Rieti Basin, central Italy), *Quat. Sci. Rev.*, 211, 186–207,
790 <https://doi.org/10.1016/j.quascirev.2019.03.004>, 2019.

791 Baranello, S., Camassi, R., and Castelli, V.: Behind the Italian catalogues: overlooked but far from negligible earthquakes,
792 *Ann. Geophys.*, 67, SE215, <https://doi.org/10.4401/ag-9096>, 2024.

793 Beck, J., Wolfers, S. and Roberts, G.P.: Bayesian earthquake dating and seismic hazard assessment using chlorine-36
794 measurements (BED v1), *Geoscientific Model Development*, 11(11), pp. 4383–4397, 2018.

795 Bemis, S. P., Micklethwaite, S., Turner, D., James, M. R., Akciz, S., Thiele, S. T., and Bangash, H. A.: Ground-based and
796 UAV-Based photogrammetry: A multi-scale, high-resolution mapping tool for structural geology and paleoseismology, *J.*
797 *Struct. Geol.*, 69, 163–178, 2014.

798 Bernardini, F., Castelli, V., Camassi, R., Caracciolo, C. H., and Ercolani, E.: A “Forgotten” Earthquake Rediscovered: the
799 1948–1949 Monti Reatini (Central Apennines) seismic sequence, *Boll. Geof. Teor. Appl.*, 54, 3, 229–244,
800 <https://doi.org/10.4430/bgta0113>, 2013.

801 Blumetti, A. M., Dramis, F., and Michetti, A. M.: Fault generated mountain fronts in the Central Apennines (Central Italy):
802 geomorphological features and seismotectonic implications, *Earth Surf. Process. Landf.*, 18, 203–223, 1993.

803 Blumetti, A. M.: Neotectonic investigations and evidence of paleoseismicity in the epicentral area of the January–February
804 1703, Central Italy, earthquakes, in: *Perspectives in Paleoseismology*, *Bull. Assoc. Eng. Geol., Spec. Publ.* 6, 83–100, 1995.

805 Blumetti, A. M., Grützner, C., and Guerrieri, L.: Quaternary earthquakes: Geology and palaeoseismology for seismic hazard
806 assessment, *Quat. Int.*, 451, 1–10, <https://doi.org/10.1016/j.quaint.2017.04.002>, 2017.

807 Boncio, P., Lavecchia, G., Pace, B., and Visini, F.: Seismic hazard analysis for large earthquakes from a surface faulting hazard
808 perspective: the example of the 2009 L'Aquila earthquake (central Italy) and its implications for earthquake recurrence in the
809 Apennines, *Tectonophysics*, 522–523, 33–45, <https://doi.org/10.1016/j.tecto.2011.12.014>, 2012.

810 Borrelli, P., Domdey, C., Hoelzmann, P., Knitter, D., Panagos, P., and Schütt, B.: Geoarchaeological and historical
811 implications of late Holocene landscape development in the Carseolani Mountains, central Apennines, Italy, *Geomorphology*,
812 216, 26–39, 2014.

813 Bosi, C.: Osservazioni preliminari su faglie probabilmente attive nell'Appennino centrale, *Boll. Soc. Geol. It.*, 94, 4, 827–859,
814 1975.

815 Brunamonte, F., Michetti, A. M., Serva, L., and Vittori, E.: Seismic-hazard evaluation in Central Italy: preliminary results of
816 the Rieti Basin project, *Ann. Geophys.*, 36, 21, <https://doi.org/10.4401/ag-4309>, 1993.

817 Brunamonte, F., Michetti, A. M., Guerrieri, L., and Serva, L.: L'evoluzione tardo-quaternaria del Bacino di Rieti e la
818 formazione del Lacus Velinus, in: Virili, C. (Ed.), *Atti Giornata di Studi sulla Protostoria nell'area del Lacus Velinus*, Rieti,
819 12 Dicembre 2009, Teseo Editore, Roma, 59–88, ISBN 978-88-95291-17-8, 2022.

820 Calderini, G., Calderoni, G., Cavinato, G. P., Gliozzi, E., and Paccara, P.: The upper Quaternary sedimentary sequence at the
821 Rieti Basin (central Italy): a record of sedimentation response to climatic changes, *Palaeogeogr. Palaeoclimatol. Palaeoecol.*,
822 140, 97–111, 1998.

823 Capotorti, F., and Muraro, C.: Jurassic to Quaternary reactivation of inherited structures in the central Apennines, Ital. J.
824 Geosci., 143, 37–59, <https://doi.org/10.3301/IJG.2024.03>, 2024.

825 Carrara, C., Brunamonte, F., Ferreli, L., Lorenzoni, P., Margheriti, L., Michetti, A. M., Raglione, M., Rosati, M., and Serva,
826 L.: I terrazzi della medio-bassa valle del F. Velino, Studi Geol. Camerti, Spec. Vol. 1992/1, 97–102, 1992.

827 Cavinato, G. P.: Controls and stratigraphic implications of synsedimentary tectonics in Plio–Quaternary continental deposits
828 of the Roman Basin, central Italy, Geol. Romana, 29, 81–100, 1993.

829 Cavinato, G. P., Carusi, C., Dall’Asta, M., Miccadei, E., and Piacentini, T.: Sedimentary and tectonic evolution of Plio–
830 Pleistocene alluvial and lacustrine deposits of Fucino Basin (central Italy), Sediment. Geol., 148, 29–59, 2002.

831 Cavinato, G. P., and De Celles, P. D.: Extensional basins in the tectonically bimodal central Apennines fold-thrust belt, Italy:
832 response to corner flow above a subducting slab in retrograde motion, Geology, 27, 955–958, 1999.

833 Cavinato, P., Gliozzi, E., and Mazzini, I.: Two lacustrine episodes during the Late Pliocene–Holocene evolution of the Rieti
834 Basin (Central Apennines, Italy), AAPG Stud. Geol., 46, 527–534, 2000.

835 Cinti, F. R., Civico, R., Blumetti, A. M., Chiarini, E., La Posta, E., Pantosti, D., Papasodaro, F., Smedile, A., De Martini, P.
836 M., and Villani, F.: Evidence for surface faulting earthquakes on the Montereale fault system (Abruzzi Apennines, central
837 Italy), Tectonics, 37, 2758–2776, <https://doi.org/10.1029/2018TC005054>, 2018.

838 Cinti, F. R., De Martini, P. M., Pantosti, D., Baize, S., Smedile, A., Villani, F., et al.: 22-kyr-long record of surface faulting
839 along the source of the 30 October 2016 earthquake (central Apennines, Italy), from integrated paleoseismic data sets. Journal
840 of Geophysical Research: Solid Earth, 124, <https://doi.org/10.1029/2019JB017757>, 2019.

841 Cinti, F. R., Pantosti, D., De Martini, P. M., Pucci, S., Civico, R., Pierdominici, S., and Patera, A.: Evidence for surface faulting
842 events along the Paganica fault prior to the 6 April 2009 L’Aquila earthquake (central Italy), J. Geophys. Res.-Sol. Ea., 116,
843 B7, <https://doi.org/10.1029/2010JB007998>, 2011.

844 Comerci, V., Molin, D., Pasquaré, F. A., and Serva, L.: Risposta sismica dell’area urbana di Rieti in occasione del terremoto
845 del 27 giugno 1898 nel bacino di Vazia (RI), Boll. Soc. Geol. It., 122, 147–156, 2003.

846 Commissione tecnica per la microzonazione sismica: Linee guida per la gestione del territorio in aree interessate da Faglie
847 Attive e Capaci (FAC), versione 1.0, Conferenza delle Regioni e delle Province Autonome – Dipartimento della Protezione
848 Civile, Roma, 66 pp., <https://www.protezionecivile.gov.it/it/pubblicazione/microzonazione-sismica-linee-guida-per-la-gestione-del-territorio-in-aree-interessate-da-faglie-attive-e-capaci--fac-/>, 2015.

849

850 Cosentino, D., Cipollari, P., Marsili, P., and Scrocca, D.: Geology of the central Apennines: a regional review, J. Virtual
851 Explor., 36, 1–37, 2010.

852 Cowie, P. A. and Roberts, G. P.: Constraining slip rates and spacings for active normal faults, J. Struct. Geol., 23, 1901–1915,
853 [https://doi.org/10.1016/S0191-8141\(01\)00036-0](https://doi.org/10.1016/S0191-8141(01)00036-0), 2001.

854 Crone, A. J., Machette, M. N., Bonilla, M. G., Lienkaemper, J. J., Pierce, K. L., Scott, W. E., and Bucknam, R. C.: Surface
855 faulting accompanying the Borah Peak earthquake and segmentation of the Lost River fault, central Idaho. *Bulletin of the
856 Seismological Society of America*, 77(3), 739–770, 1987.

857 Dahlin, T., and Zhou, B. A numerical comparison of 2D resistivity imaging with 10 electrode arrays. Geophysical prospecting,
858 52(5), 379–398, 2004

859 Destro, N.: Release fault: A variety of cross fault in linked extensional fault systems, in the Sergipe-Alagoas Basin, NE Brazil,
860 J. Struct. Geol., 17, 615–629, [https://doi.org/10.1016/0191-8141\(94\)00100-X](https://doi.org/10.1016/0191-8141(94)00100-X), 1995.

861 Di Domenica, A. and Pizzi, A.: Defining a mid-Holocene earthquake through speleoseismological and independent data:
862 implications for the outer Central Apennines (Italy) seismotectonic framework, Solid Earth, 8, 161–176,
863 <https://doi.org/10.5194/se-8-161-2017>, 2017.

864 Doglioni, C.: A proposal for the kinematic modelling of W-dipping subductions—possible implications for the Apennines–
865 Maghrebides and the Alps, Terra Nova, 3, 423–434, <https://doi.org/10.1111/j.1365-3121.1991.tb00172.x>, 1991.

866 Doser, D. I.: Source parameters and faulting processes of the August 1959 Hebgen Lake, Montana earthquake sequence, Ph.D.
867 thesis, The University of Utah, USA, 1984.

868 Doser, D. I.: Earthquake processes in the Rainbow Mountain–Fairview Peak–Dixie Valley, Nevada, region 1954–1959, J.
869 Geophys. Res.–Sol. Ea., 91, 12572–12586, <https://doi.org/10.1029/JB091iB12p12572>, 1986.

870 Dramis, F.: Il ruolo dei sollevamenti tettonici a largo raggio nella genesi del rilievo appenninico, Studi Geol. Camerti, 1, 9–
871 15, 1992.

872 Faure Walker, J., Boncio, P., Pace, B., Roberts, G., Benedetti, L., Scotti, O., Visini, F., and Peruzza, L.: Fault2SHA Central
873 Apennines database and structuring active fault data for seismic hazard assessment, Sci. Data, 8, 87,
874 <https://doi.org/10.1038/s41597-021-00864-0>, 2021.

875 Galadini, F. and Galli, P.: The Holocene paleoearthquakes on the 1915 Avezzano earthquake faults (central Italy): implications
876 for active tectonics in the central Apennines, Tectonophysics, 308, 143–170, [https://doi.org/10.1016/S0040-1951\(99\)00103-9](https://doi.org/10.1016/S0040-1951(99)00103-9), 1999.

877 Galadini, F., Messina, P., Giaccio, B., and Sposato, A.: Early uplift history of the Abruzzi Apennines (central Italy): available
878 geomorphological constraints, Quat. Int., 101, 125–135, [https://doi.org/10.1016/S1040-6182\(02\)00132-7](https://doi.org/10.1016/S1040-6182(02)00132-7), 2003.

879 Galli, P., Galadini, F., and Pantosti, D.: Twenty years of paleoseismology in Italy, Earth-Sci. Rev., 88, 89–117,
880 <https://doi.org/10.1016/j.earscirev.2008.01.001>, 2008.

881 Galli, P. A., Giaccio, B., Messina, P., Peronace, E., and Zuppi, G. M.: Palaeoseismology of the L’Aquila faults (central Italy,
882 2009, M w 6.3 earthquake): implications for active fault linkage, Geophys. J. Int., 187, 1119–1134,
883 <https://doi.org/10.1111/j.1365-246X.2011.05197.x>, 2011.

884 Galli, P., Castenetto, S., and Peronace, E.: The macroseismic intensity distribution of the 30 October 2016 earthquake in central
885 Italy (Mw 6.6): Seismotectonic implications, Tectonics, 36, 2179–2191, <https://doi.org/10.1002/2017TC004653>, 2017.

886 Galli, P., Galderisi, A., Martino, M., Scarascia Mugnozza, G., and Bozzano, F.: The coseismic faulting of the San Benedetto
887 tunnel (2016, Mw 6.6 central Italy earthquake), in: Tunnels and Underground Cities: Engineering and Innovation Meet
888 Archaeology, Architecture and Art, edited by: Peila, Viggiani and Celestino, 805–811, Taylor & Francis Group, London, ISBN
889 978-1-38-38865-9, 2020.

890 Galli, P., Galderisi, A., Peronace, E., Giaccio, B., Hajdas, I., Messina, P., Pieaggi, D. and Polpetta, F.: The awakening of the
891 dormant Mount Vettore fault (2016 central Italy earthquake, Mw 6.6): Paleoseismic clues on its millennial silences. Tectonics,
892 38(2), 687–705, 2019.

893 Galli, P., Peronace, E., and Messina, P.: Archaeoseismic evidence of surface faulting in 1703 Norcia earthquake (Central
894 Italian Apennines, Mw 6.9), Geosciences, 12, 14, <https://doi.org/10.3390/geosciences12010014>, 2021.

896 Galluzzo, F. and Santantonio, M.: The Sabina Plateau: a new element in the Mesozoic paleogeography of Central Apennines,
897 Boll. Soc. Geol. Ital., 1, 561–588, 2002.

898 Giardini, D.: Teleseismic observation of the November 23, 1980, Irpinia earthquake, Ann. Geophys., 36, 1, 1993.

899 Gilbert, G. K.: Lake Bonneville (Vol. 1), U.S. Geol. Surv. Monogr., 1, 1438, 1890.

900 Gori, S., Falcucci, E., Di Giulio, G., Moro, M., Saroli, M., Vassallo, M., Ciampaglia, A., Di Marcantonio, P., and Trotta, D.:
901 Active Normal Faulting and Large-Scale Mass Wasting in Urban Areas: The San Gregorio Village Case Study (L'Aquila,
902 Central Italy). Methodological Insight for Seismic Microzonation Studies, Eng. Geol. for Soc. and Territ.-Vol. 5: Urban Geol.,
903 Sustain. Plan. and Landsc. Exploit., Springer, 1033–1036, 2015.

904 Gori, S., Falcucci, E., Galadini, F., Moro, M., Saroli, M., and Ceccaroni, E.: Geoarchaeology and paleoseismology blend to
905 define the Fucino active normal fault slip history, central Italy, Quaternary International 451 (2017): 114–128, 2017.

906 Guerrieri, L., Comerci, V., Ferreli, L., Pompili, R., Serva, L., Brunamonte, F., and Michetti, A. M.: Geological evolution of
907 the intermountain Rieti basin (Central Apennines), Mapping Geol. in Italy, SELCA, 123–130, 2006.

908 Guerrieri, L., Vittori, E., Comerci, V., Esposito, E., Michetti, A. M., and Porfido, S.: Ground effects and surface faulting in
909 the April 6, 2009 L'Aquila earthquake (central Italy), Nat. Hazards Earth Syst. Sci., 10, 2311–2336,
910 <https://doi.org/10.5194/nhess-10-2311-2010>, 2010.

911 Guidoboni, E., Ferrari, G., Mariotti, D., Comastri, A., Tarabusi, G., Sgattoni, G., and Valensise, G.: CFTI5Med, Catalogo dei
912 Forti Terremoti in Italia (461 a.C.-1997) e nell'area Mediterranea (760 a.C.-1500), Istituto Nazionale di Geofisica e
913 Vulcanologia (INGV), <https://doi.org/10.6092/ingv.it-cfti5>, 2018.

914 Guidoboni, E., Ferrari, G., Tarabusi, G., Sgattoni, G., Comastri, A., Mariotti, D., Ciuccarelli, C., Bianchi, M. G., and Valensise,
915 G.: CFTI5Med, the new release of the catalogue of strong earthquakes in Italy and in the Mediterranean area, Sci. Data, 6, 80,
916 <https://doi.org/10.1038/s41597-019-0091-9>, 2019.

917 Iezzi, F., Francescone, M., Pizzi, A., Blumetti, A., Boncio, P., Di Manna, P., Pace, B., Piacentini, T., Papasodaro, F., and
918 Morelli, F.: Slip localization on multiple fault splays accommodating distributed deformation across normal fault complexities,
919 Tectonophysics, 868, 230075, 2023.

920 Iezzi, F., Roberts, G., Walker, J. F., and Papanikolaou, I.: Occurrence of partial and total coseismic ruptures of segmented
921 normal fault systems: Insights from the Central Apennines, Italy, J. Struct. Geol., 126, 83–99, 2019.

922 Liotier, Y.: Modelisation des ondes de volume des seismes se l'arc Ageoen, DEA de l'Universite Joseph Fourier, Grenoble,
923 France, 1989 (in French).

924 Lombardi, A. M., Cinti, F. R., and Pantosti, D.: Paleoearthquakes modeling and effects of uncertainties on probability
925 assessment of next fault ruptures: the case of Central Italy surface faulting earthquakes, Geophys. J. Int., 2025; ggaf105,
926 <https://doi.org/10.1093/gji/ggaf105>, 2025.

927 Lorenzoni, P., Raglione, M., Brunamonte, F., Michetti, A. M., and Pennacchioni, M.: Stratigrafia dei depositi di versante tardo-
928 quaternari del Bacino di Rieti: la sezione de "La Casetta", Studi Geol. Camerti, Spec. Vol. 1992/1, 145–153, 1993.

929 Lustrino, M., Pistocchi, L., Ronca, S., Innocenzi, F., and Agostini, S.: Origin of ultrapotassic, ultracalcic, ultrabasic SiO₂-
930 undersaturated magmas: The case study of the Pleistocene Cupaello kamafugite monogenetic volcano, central Italy, Geochem.
931 Geophys. Geosyst., 26, e2024GC011683, <https://doi.org/10.1029/2024GC011683>, 2025.

932 Maceroni, D., Dixit Dominus, G., Gori, S., Falcucci, E., Galadini, F., Moro, M., and Saroli, M.: First evidence of the Late
933 Pleistocene—Holocene activity of the Roveto Valley Fault (Central Apennines, Italy), *Frontiers in Earth Science*, 10, 1018737,
934 2022.

935 McCalpin, J. P.: Paleoseismology in extensional tectonic environments, *Int. Geophys.*, 95, 171–269, 2009.

936 Messina, P., Galadini, F., Galli, P., and Sposato, A.: Quaternary basin evolution and present tectonic regime in the area of the
937 1997–1998 Umbria–Marche seismic sequence (central Italy), *Geomorphology*, 42(1-2), 97–116, 2002.

938 Michetti, A. M., Brunamonte, F., Serva, L., and Whitney, R. A.: Seismic hazard assessment from paleoseismological evidence
939 in the Rieti Region (Central Italy), *Perspect. Paleoseismol., Assoc. Eng. Geol. Bull., Special Publ.*, 63–82, 1995.

940 Michetti, A. M., Brunamonte, F., Serva, L., and Vittori, E.: Trench investigations of the 1915 Fucino earthquake fault scarps
941 (Abruzzo, Central Italy): geological evidence of large historical events, *J. Geophys. Res. Solid Earth*, 101, 5921–5936, 1996.

942 Mildon, Z. K., Roberts, G. P., Faure Walker, J. P., and Iezzi, F.: Coulomb stress transfer and fault interaction over millennia
943 on non-planar active normal faults: The M w 6.5–5.0 seismic sequence of 2016–2017, central Italy, *Geophys. J. Int.*, 210(2),
944 1206–1218, 2017.

945 Mildon, Z. K., Roberts, G. P., Faure Walker, J. P., Beck, J., Papanikolaou, I., Michetti, A. M., and Vittori, E.: Surface faulting
946 earthquake clustering controlled by fault and shear-zone interactions, *Nat. Commun.*, 13(1), 7126, 2022.

947 Moderni, P.: Il terremoto di Rieti del 28 giugno 1898, *Bollett. Regio Comit. Geol. Italia*, 30(3), 263–268, 1899.

948 Moro, M., Falcucci, E., Gori, S., Saroli, M., and Galadini, F.: New paleoseismic data across the Mt. Marine Fault between the
949 2016 Amatrice and 2009 L’Aquila seismic sequences (central Apennines), *Ann. Geophys.*, 2016.

950 Mouslopoulou, V., Nicol, A., Howell, A., and Griffin, J. D.: Comparison of paleoearthquake elapsed-times and mean
951 interevent-times for a global data set of active faults: Implications for future earthquakes and seismic hazard, *J. Geophys. Res.
952 Solid Earth*, 130, e2024JB030036, <https://doi.org/10.1029/2024JB030036>, 2025.

953 Obsequens Iulius: *Prodigiorum liber*, in "T. Livi Periochae omnium librorum. Fragmenta Oxyrhynchi reperta. Iulii Obsequentis
954 Prodigiorum liber", ed. O. Rossbach, pp.149-181, *Bibliotheca scriptorum Graecorum et Romanorum Teubneriana*, Leipzig,
955 1910.

956 Pantosti, D., D’Addazio, G., and Cinti, F. R.: Paleoseismicity of the Ovindoli-Pezza fault, central Apennines, Italy: A history
957 including a large, previously unrecorded earthquake in the Middle Ages (860–1300 AD), *J. Geophys. Res. Solid Earth*, 101,
958 5937–5959, 1996.

959 Pantosti, D., and Valensise, G.: Faulting mechanism and complexity of the November 23, 1980, Campania-Lucania
960 earthquake, inferred from surface observations, *J. Geophys. Res. Solid Earth*, 95, 15319–15341,
961 <https://doi.org/10.1029/JB095iB10p15319>, 1990.

962 Papanikolaou, I. D., and Roberts, G. P.: Geometry, kinematics and deformation rates along the active normal fault system in
963 the southern Apennines: Implications for fault growth, *J. Struct. Geol.*, 29(1), 166–188, 2007.

964 Pavlides, S., and Caputo, R.: Magnitude versus faults' surface parameters: quantitative relationships from the Aegean
965 Region, *Tectonophysics*, 380(3-4), 159–188, 2004.

966 Porreca, M., Fabbrizzi, A., Azzaro, S., Pucci, S., Del Rio, L., Pierantoni, P. P., and Barchi, M. R.: 3D geological reconstruction
967 of the M. Vettore seismogenic fault system (Central Apennines, Italy): Cross-cutting relationship with the M. Sibillini thrust,
968 *J. Struct. Geol.*, 131, 103938, 2020.

969 Pousse-Beltran, L., Benedetti, L., Fleury, J., Boncio, P., Guillou, V., Pace, B., Rizza M., Puliti I., Socquet A. and Aster Team:
970 36Cl exposure dating of glacial features to constrain the slip rate along the Mt. Vettore Fault (Central Apennines, Italy).
971 *Geomorphology*, 412, 108302, 2022.

972 Pucci, S., De Martini, P. M., Civico, R., Villani, F., Nappi, R., Ricci, T., Azzaro, R., Brunori, C. A., Caciagli, M., Cinti, F. R.,
973 Sapia, V., De Ritis, R., Mazzarini, F., Tarquini, S., Gaudiosi, G., Nave, R., Alessio, G., Smedile, A., Alfonsi, L., Cucci, L.,
974 and Pantosti, D.: Coseismic ruptures of the 24 August 2016, Mw 6.0, Amatrice earthquake (central Italy), *GSA Today*, 27, 4–
975 10, <https://doi.org/10.1130/GSATG321A.1>, 2017.

976 Puliti, I., Benedetti, L., Pizzi, A., Fleury, J., Francescone, M., Guillou, V., and Aster Team: Evidence for a constant slip rate
977 over the last ~40 ka along the Mt. Morrone fault system in Central Apennines, *Tectonics*, 43(3), e2023TC007871, 2024.

978 Puliti, I., Pizzi, A., Benedetti, L., Di Domenica, A., and Fleury, J.: Comparing slip distribution of an active fault system at
979 various timescales: Insights for the evolution of the Mt. Vettore-Mt. Bove fault system in Central Apennines. *Tectonics*, 39(9),
980 e2020TC006200, 2020.

981 Roberts, G. P., and Michetti, A. M.: Spatial and temporal variations in growth rates along active normal fault systems: an
982 example from the Lazio–Abruzzo Apennines, central Italy, *J. Struct. Geol.*, 26, 339–376, 2004.

983 Roberts, G. P., Iezzi, F., Sgambato, C., Robertson, J., Beck, J., Mildon, Z. K., Papanikolaou, I., Michetti, A. M., Faure Walker,
984 J. P., Mitchell, S., Meschis, M., Shanks, R. P., Phillips, R., McCaffrey, K., Vittori, E., Visini, F., and Iqbal, M.: Characteristics
985 and modelling of slip-rate variability and temporal earthquake clustering across a distributed network of active normal faults
986 constrained by in situ 36Cl cosmogenic dating of fault scarp exhumation, central Italy, *J. Struct. Geol.*, 195, 105391,
987 <https://doi.org/10.1016/j.jsg.2025.105391>, 2025.

988 Rovida, A., Locati, M., Camassi, R., Lolli, B., Gasperini, P., and Antonucci, A. (eds): Italian Parametric Earthquake Catalogue
989 (CPTI15), version 4.0, Istituto Nazionale di Geofisica e Vulcanologia (INGV), <https://doi.org/10.13127/cpti/cpti15.4>, 2022.

990 Salvi, S., Cinti, F. R., Colini, L., D’Addezio, G., Doumaz, F., and Pettinelli, E.: Investigation of the active Celano–L’Aquila
991 fault system, Abruzzi (central Apennines, Italy) with combined ground-penetrating radar and palaeoseismic trenching,
992 *Geophys. J. Int.*, 155, 805–818, 2003.

993 Santantonio, M., and Carminati, E.: Jurassic rifting evolution of the Apennines and Southern Alps (Italy): Parallels and
994 differences, *Bull.*, 123, 468–484, 2011.

995 Scognamiglio, L., Tinti, E., Casarotti, E., Pucci, S., Villani, F., Cocco, M., Magnoni, F., Michelini, A., Dreger, D.: Complex
996 fault geometry and rupture dynamics of the MW 6.5, 30 October 2016, Central Italy earthquake. *Journal of Geophysical
997 Research: Solid Earth* 123, 2943–2964, 2018.

998 Scotti, O., Visini, F., Faure Walker, J., Peruzza, L., Pace, B., Benedetti, L., Boncio, P., and Roberts, G.: Which Fault Threatens
999 Me Most? Bridging the Gap Between Geologic Data-Providers and Seismic Risk Practitioners, *Front. Earth Sci.*, 8, 626401,
1000 <https://doi.org/10.3389/feart.2020.626401>, 2021.

1001 Serva, L., Michetti, A. M., and Trippa, G.: Trench investigations across the 1915 surface faulting in the Fucino Basin (central
1002 Italy), *Mem. Soc. Geol. It.*, 35, 893–907, 1986.

1003 Slemmons, D. B.: Geological effects of the Dixie valley-Fairview peak, Nevada, earthquakes of December 16, 1954, *Bull.
1004 Seismol. Soc. Am.*, 47(4), 353–375, 1957.

1005 Servizio Geologico d’Italia (in press) - Carta geologica d’Italia alla scala 1:50.000, F. 347 Rieti. ISPRA. Roma.

1006 Tucker, G. E., McCoy, S. W., Whittaker, A. C., Roberts, G. P., Lancaster, S. T., and Phillips, R.: Geomorphic significance of
1007 postglacial bedrock scarps on normal-fault footwalls. *Journal of Geophysical Research: Earth Surface*, 116, F01022, 1-14,
1008 doi:10.1029/2010JF001861, 2011.

1009 Valentini, G., Volatili, T., Galli, P., and Tondi, E.: A millennial perspective on Coulomb stress transfer impact in the seismicity
1010 of the Central Apennine Fault System, EGU General Assembly 2024, Vienna, Austria, 14–19 Apr 2024, EGU24-7956,
1011 <https://doi.org/10.5194/egusphere-egu24-7956>, 2024.

1012 Villani, F., Civico, R., Pucci, S., Pizzimenti, L., Nappi, R., De Martini, P. M., and the Open Emergeo Working Group: A
1013 database of the coseismic effects following the 30 October 2016 Norcia earthquake in Central Italy, *Sci. Data*, 5(1), 1–11,
1014 2018.

1015 Wells, D. L., and Coppersmith, K. J.: New empirical relationships among magnitude, rupture length, rupture width, rupture
1016 area, and surface displacement. *Bulletin of the seismological Society of America*, 84(4), 974–1002, 1994.

1017 Westoby, M. J., Brasington, J., Glasser, N. F., Hambrey, M. J., and Reynolds, J. M.: ‘Structure-from-Motion’ photogrammetry:
1018 A low-cost, effective tool for geoscience applications, *Geomorphology*, 179, 300–314, 2012.

1019